



Department for
Business, Energy
& Industrial Strategy

Primary Store Geological Model & Report

Key Knowledge Document

NS051-SS-REP-000-00014

August 2021

Acknowledgements

The information in this report has been prepared by bp on behalf of itself and its partners on the Northern Endurance Partnership project for review by the Department of Business, Energy and Industrial Strategy (“BEIS”) only. While bp believes the information and opinions given in this report to be sound, all parties must rely upon their own skill and judgement when making use of it. By sharing this report with BEIS, neither bp nor its partners on the Northern Endurance Partnership project make any warranty or representation as to the accuracy, completeness, or usefulness of the information contained in the report, or that the same may not infringe any third party rights. Without prejudice to the generality of the foregoing sentences, neither bp nor its partners represent, warrant, undertake or guarantee that the outcome or results referred to in the report will be achieved by the Northern Endurance Partnership project. Neither bp nor its partners assume any liability for any loss or damages that may arise from the use of or any reliance placed on the information contained in this report.

© BP Exploration Operating Company Limited 2021. All rights reserved.



© Crown copyright 2021

This publication is licensed under the terms of the Open Government Licence v3.0 except where otherwise stated. To view this licence, visit nationalarchives.gov.uk/doc/open-government-licence/version/3 or write to the Information Policy Team, The National Archives, Kew, London TW9 4DU, or email: psi@nationalarchives.gsi.gov.uk.

Where we have identified any third-party copyright information you will need to obtain permission from the copyright holders concerned.

Any enquiries regarding this publication should be sent to us at: enquiries@beis.gov.uk

Contents

| | |
|-----------------------------------------------------------------------|----|
| Foreword | 5 |
| Executive Summary | 7 |
| 1.0 Introduction | 9 |
| 1.1 Purpose | 9 |
| 1.2 Location | 10 |
| 1.3 Geological Setting | 10 |
| 1.3.1 Structural and Stratigraphic Evolution | 11 |
| 1.3.1.1 Ordovician to Carboniferous | 14 |
| 1.3.1.2 Permian | 14 |
| 1.3.1.3 Triassic | 15 |
| 1.3.1.4 Jurassic to Early Cretaceous | 15 |
| 1.3.1.5 Late Cretaceous to Cenozoic | 15 |
| 1.4 Exploration and Appraisal History | 16 |
| 1.5 Storage Site and Storage Complex | 16 |
| 2.0 Reservoir Characterisation: Sedimentology of the Bunter Sandstone | 19 |
| 2.1 Previous work | 19 |
| 2.2 Lithotype Core Study | 19 |
| 2.3 Core Overview | 19 |
| 2.4 Lithotypes Guide | 20 |
| 2.5 Depositional Environment Interpretation | 25 |
| 2.6 Analogues and Implications for Modelling | 25 |
| 2.7 Surfaces/transmissibility Barriers | 27 |
| 2.7.1 Cements | 27 |
| 2.7.1.1 Crumbly Cement/crust | 27 |
| 2.7.1.2 Patchy Bleached Cement | 27 |
| 2.7.1.3 Cemented Surfaces | 28 |
| 2.7.2 Heterolithics | 28 |
| 2.7.2.1 Silty Mud-crack Surfaces | 28 |
| 2.8 Potential Facies Types | 29 |
| 2.9 Lithotype Rock Properties Variation | 30 |

| | |
|----------------------------------------------------|----|
| 3.0 Petrophysical Model | 32 |
| 3.1 Data Inventory | 32 |
| 3.1.1 Volume of Clay (VCL) | 33 |
| 3.1.2 Porosity | 33 |
| 3.1.3 Permeability | 34 |
| 3.1.4 Net Reservoir | 35 |
| 3.1.5 Property Summary | 35 |
| 4.0 Seal Characterisation | 37 |
| 5.0 Static Modelling | 43 |
| 5.1 Introduction | 43 |
| 5.2 Area of Interest | 43 |
| 5.3 Structural Model | 45 |
| 5.3.1 Fault Modelling | 46 |
| 5.3.2 Create Simple Grid | 46 |
| 5.3.3 Horizon Modelling/Make Horizons | 46 |
| 5.3.4 Zone Modelling/Make zone | 46 |
| 5.3.5 Layering | 47 |
| 5.4 Grid | 48 |
| 5.4.1 Well Log Upscaling | 48 |
| 5.5 Facies Modelling | 48 |
| 5.5.1 Variograms Derived from Lithotype Core Study | 50 |
| 5.6 Petrophysical Modelling | 54 |
| 5.6.1 Net-to-Gross (NTG) | 54 |
| 5.6.2 Porosity | 54 |
| 5.6.3 Permeability | 57 |
| 5.7 Upscaling | 59 |
| 5.8 Static Model QC | 61 |
| 5.9 Fault and Segment | 63 |
| 5.10 Volumetrics | 64 |
| 6.0 Conclusions | 65 |
| 7.0 References | 67 |

Foreword

The Net Zero Teesside (NZN) project in association with the Northern Endurance Partnership project (NEP) intend to facilitate decarbonisation of the Humber and Teesside industrial clusters during the mid-2020s. Both projects will look to take a Final Investment Decision (FID) in early 2023, with first CO₂ capture and injection anticipated in 2026.

The projects address widely accepted strategic national priorities – most notably to secure green recovery and drive new jobs and economic growth. The Committee on Climate Change (CCC) identified both gas power with Carbon Capture, Utilisation and Storage (CCUS) and hydrogen production using natural gas with CCUS as critical to the UK's decarbonisation strategy. Gas power with CCUS has been independently estimated to reduce the overall UK power system cost to consumers by £19bn by 2050 (compared to alternative options such as energy storage).

Net Zero Teesside Onshore Generation & Capture

NZN Onshore Generation & Capture (G&C) is led by bp and leverages world class expertise from ENI, Equinor, and TotalEnergies. The project is anchored by a world first flexible gas power plant with CCUS which will compliment rather than compete with renewables. It aims to capture ~2 million tonnes of CO₂ annually from 2026, decarbonising 750MW of flexible power and delivering on the Chancellor's pledge in the 2020 Budget to "support the construction of the UK's first CCUS power plant." The project consists of a newbuild Combined Cycle Gas Turbine (CCGT) and Capture Plant, with associated dehydration and compression for entry to the Transportation & Storage (T&S) system.

Northern Endurance Partnership Onshore/Offshore Transportation & Storage

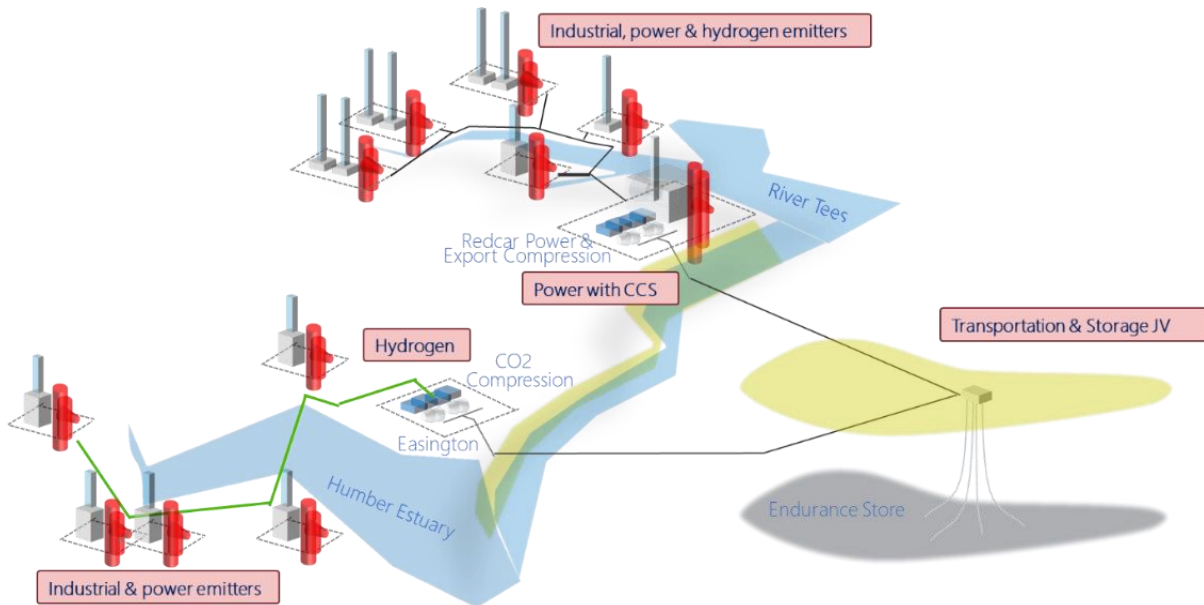
The NEP brings together world-class organisations with the shared goal of decarbonising two of the UK's largest industrial clusters: the Humber (through the Zero Carbon Humber (ZCH) project), and Teesside (through the NZN project). NEP T&S includes the G&C partners plus Shell, along with National Grid, who provide valuable expertise on the gathering network as the current UK onshore pipeline transmission system operator.

The Onshore element of NEP will enable a reduction of Teesside's emissions by one third through partnership with industrial stakeholders, showcasing a broad range of decarbonisation technologies which underpin the UK's Clean Growth strategy and kickstarting a new market for CCUS. This includes a new gathering pipeline network across Teesside to collect CO₂ from industrial stakeholders towards an industrial Booster Compression system, to condition and compress the CO₂ to Offshore pipeline entry specification.

Offshore, the NEP project objective is to deliver technical and commercial solutions required to implement innovative First-of-a-Kind (FOAK) offshore low-carbon CCUS infrastructure in the UK, connecting the Humber and Teesside Industrial Clusters to the Endurance CO₂ Store in the Southern North Sea (SNS). This includes CO₂ pipelines connecting from Humber and Teesside compression/pumping systems to a common subsea manifold and well injection site

at Endurance, allowing CO₂ emissions from both clusters to be transported and stored. The NEP project meets the CCC's recommendation and HM Government's Ten Point Plan for at least two clusters storing up to 10 million tonnes per annum (Mtpa) of CO₂ by 2030.

TEESSIDE (NZT)



HUMBERSIDE (ZHC)

NEP

The project initially evaluated two offshore CO₂ stores in the SNS: 'Endurance', a saline aquifer formation structural trap, and 'Hewett', a depleted gas field. The storage capacity requirement was for either store to accept 6+ Mtpa CO₂ continuously for 25 years. The result of this assessment after maturation of both options, led to Endurance being selected as the primary store for the project. This recommendation is based on the following key conclusions:

- The storage capacity of Endurance is 3 to 4 times greater than that of Hewett
- The development base cost for Endurance is estimated to be 30 to 50% less than Hewett
- CO₂ injection into a saline aquifer is a worldwide proven concept, whilst no benchmarking is currently available for injection in a depleted gas field in which Joule-Thompson cooling effect has to be managed via an expensive surface CO₂ heating solution.

Following selection of Endurance as the primary store, screening of additional stores has been initiated to replace Hewett by other candidates. Development scenarios incorporating these additional stores will be assessed as an alternative to the sole Endurance development.

Executive Summary

Sedimentological and rock property studies have been conducted for the Endurance structure to geologically and petrophysically characterise the subsurface, focussing on the Triassic Bunter Sandstone reservoir interval. The Bunter Sandstone was deposited in a semi-arid, landlocked, gradually subsiding basin with fluvial systems terminating in playa lake, playa margin, aeolian dune and sabkha settings. A detailed sedimentological lithotyping study was conducted for this project, focus on identifying potential baffle/barrier lithotypes and understanding their deposition to underpin their distribution within the static model.

Cores from well 42/25d-3 were interpreted to reflect an overall fluvial-aeolian setting, with highly reworked depositional elements. The effect is of an amalgam of remnant dunes, small-scale stream channels, splays and rare interfluves in a highly reworked, low accommodation space setting. It is unlikely that any one depositional element is completely preserved, and therefore dimensional width/thickness relationships are unlikely to apply. Baffles identified in the core that are likely to have lateral extent are cm to ~10 cm silty layers, that often form half-m scale heterolithic units. Their lateral extent is dependent on their depositional environment interpretation: interfluvial settings, margins of a playa lake or stratigraphic surface associated with shifts in climate or sediment supply. The sedimentological interpretation of the extent of possible baffles at Endurance was incorporated into the static models via variograms, which included a range to test sensitivities.

The petrophysical model was created to provide the rock property inputs to the static model, using data from the three wells drilled on structure and supplemented with off-structure wells to provide appropriate property ranges. The mean average properties on structure indicate that the Bunter Sandstone is a very high net to gross system, with good porosity and permeability reservoir quality. Expected parameter ranges (P10 – Mean – P90) are: net-to-gross 74 – 95 – 97%; porosity 16.4 – 22.5 – 24.1% and permeability 100 – 300 – 500mD (based on net reservoir cut-offs of $V_{cl} < 0.2$ and porosity > 0.1). Outside of structure (and seismic phase reversal), wells show varying degrees of halite cementation that can be flagged from log data.

A set of static models was built in Petrel that capture the uncertainty (overall level of vertical and horizontal heterogeneities) and honour the dynamic data. The models incorporated the insights from the core lithotype study, reprocessed seismic data and regional analogues. Emphasis was placed in building a fine grid that could capture the vertical heterogeneities observed in the core. A fine-scale grid was built at near log scale resolution. Four petrofacies (cemented sandstone, partially cemented sandstone, good-quality sandstone, and heterolithics) and five potentially continuous baffled zones were distributed across the reservoir, honouring the gross areas of cemented and un-cemented rock based on the seismic phase reversal (SPR). Porosity was modelled per facies via a gaussian simulation process and permeability was directly calculated from modelled porosity using a porosity-permeability transform (adjusted to match the dynamic data from well test in 42/25d-3). Reservoir properties were upscaled back to coarse-scale model (simulation grid) using a flow-based upscaling algorithm. The integration of geophysical, geological and petrophysical studies have enabled

the building of geologically realistic models that capture subsurface uncertainty and can be used as a tool to quantify the impact on CO₂ injection and brine offtake scenarios.

1.0 Introduction

The Endurance structure in the Southern North Sea is one of several saline aquifer structures that have been identified as potentially suitable storage sites for CCUS. This report is one of a series of key knowledge documents (KKD), which describes the work program undertaken by the Net Zero Teesside & Northern Endurance Partnership (NZE/NEP) to characterise the subsurface at Endurance and create subsurface models for evaluation of CO₂ injection and storage at the Endurance CO₂ store.

1.1 Purpose

The purpose of this document is to summarize the work program completed on geological aspects of the integrated subsurface description of the Endurance store. This follows previous studies such as those completed as part of the White Rose project. Early analysis of previous studies highlighted a number of key areas to further advance understanding, which were drawn together and used in the development of the geological model used to test subsurface uncertainties and assess risk.

Subsurface storage risks can be broadly classified as those relating to containment, capacity, injectivity and monitorability, with those covered by this document focussing on injectivity, containment and capacity. Key areas to advance geological understanding to assess injectivity, containment and capacity uncertainties and risks at the Endurance store were identified as:

- Regional geology – the tectonic history of the basin, general depositional environment and variation of the Bunter Sandstone at a regional scale, diagenetic effects on brine aquifer connectivity, regional seals, analogues in the wider Southern North Sea and the petroleum charge history of the basin
- Sedimentology of the Bunter Sandstone at Endurance – reservoir-scale depositional environment and analogues, core lithotyping and identification of features of this environment that may lead to baffling and barriers within the reservoir, use of core and petrophysical logs to characterise facies and lateral extent for inclusion in static geological modelling
- Petrophysics and reservoir quality – integration of all laboratory measurements and log data, incorporating static and dynamic testing, characterisation of rock properties both of the reservoir and seals

These were investigated via geological and petrophysical studies, and in conjunction with the geophysical interpretations (see Geophysical Model KKD), led to the development of a static model based on the subsurface descriptions.

1.2 Location

The Endurance CO₂ store is situated within the United Kingdom Continental Shelf (UKCS) in the Southern North Sea (SNS), about 75 km east offshore from Flamborough Head (**Figure 1**). It straddles blocks 42/25 and 43/21 and the water depth is around 50 m. The depth to the structural crest at the top CO₂ injection interval (Bunter Sandstone Formation) is about 1000 mTVDSS.

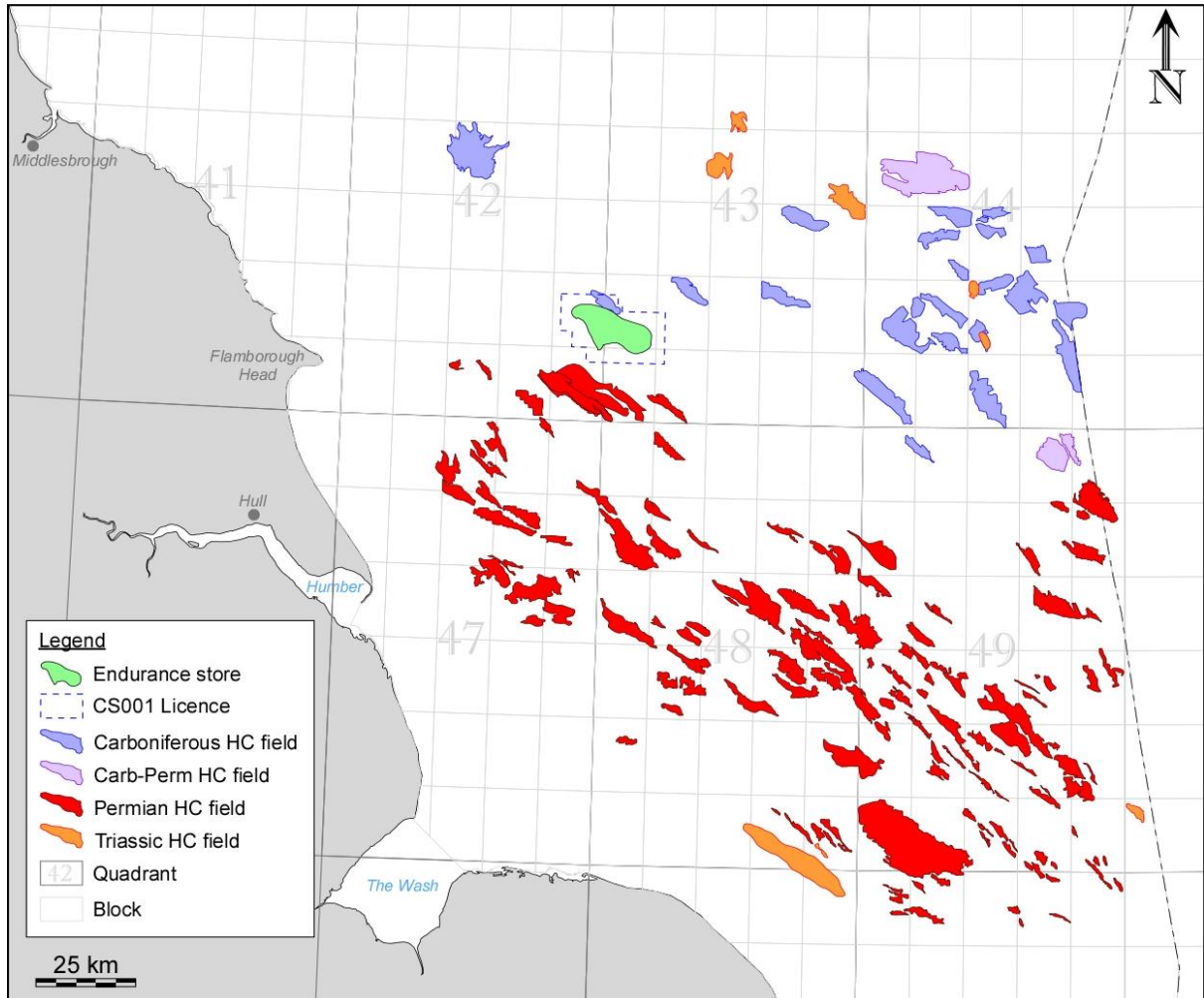


Figure 1 - Location map of the Endurance CO₂ store in the Southern North Sea.

1.3 Geological Setting

The Endurance structure is a large, four-way dip-closed anticline, formed above a salt pillow, approximately 25 km long by 8 km wide, oriented NW–SE. It is located within the Silverpit sub-basin at the western end of the much larger, E–W striking Southern Permian Basin (SPB). The basin is bound to the west by the Dowsing Fault Zone and to the east by the Cleaver Bank High. The northern limit is defined by the Mid North Sea High and the southern limit by the London-Brabant Massif (**Figure 2**).

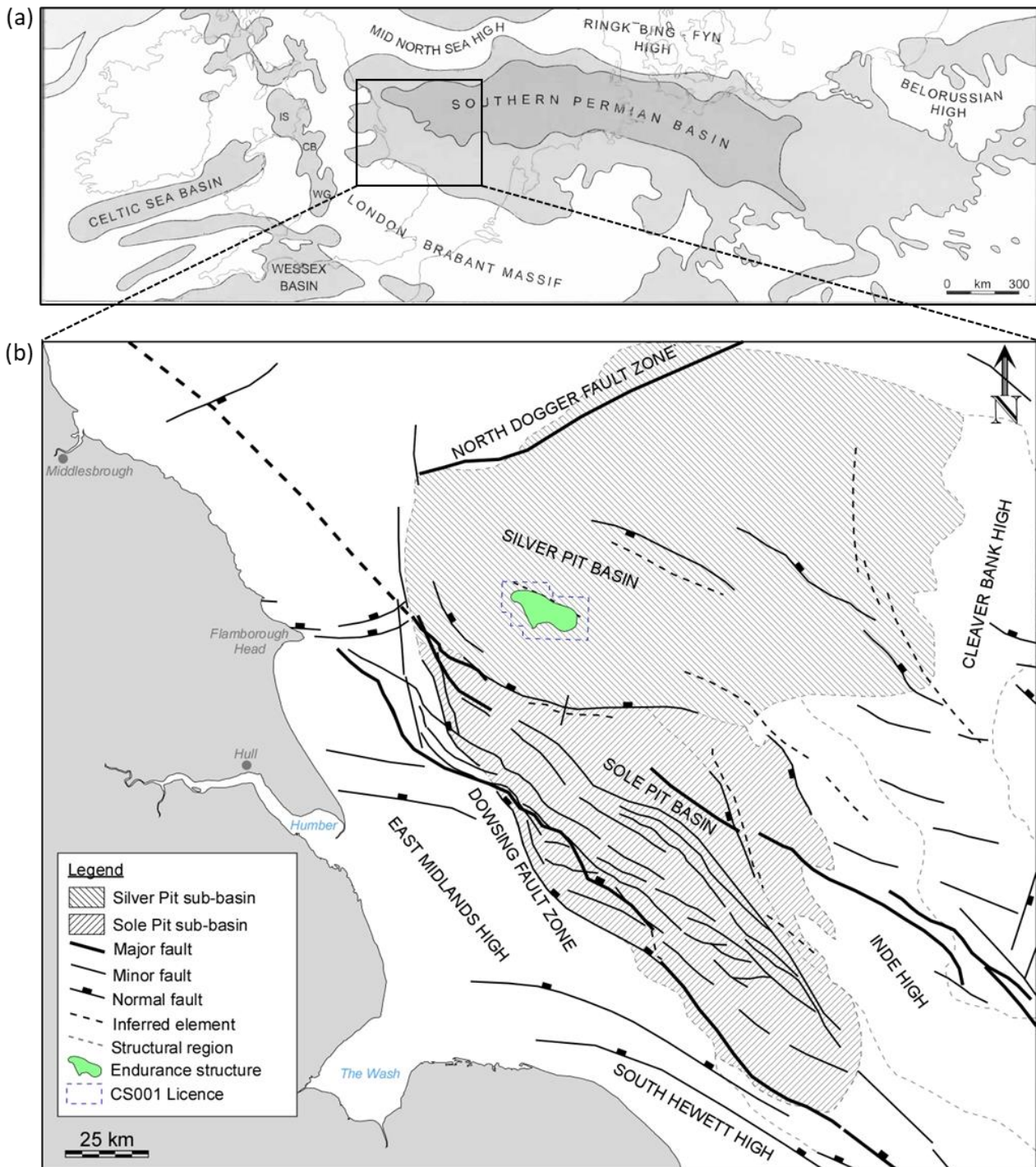


Figure 2 - Tectonic setting: (a) Extent of the Southern Permian Basin (modified from Underhill, 2003); (b) Structural elements of the Southern North Sea (modified from Richards, 2015; Pharoah et al., 2010).

1.3.1 Structural and Stratigraphic Evolution

The region has had a complex tectonic evolution but can be summarised into three key evolutionary periods: Palaeozoic continental collision and plate accretion (formation of Pangea), late Palaeozoic–Mesozoic intraplate subsidence and continental rift tectonics (break-

up of Pangea), and late Mesozoic–Cenozoic inversion and thermal uplift (Alpine Collision). The regional tectonostratigraphy of the SNS is summarised in **Figure 3** and the lithostratigraphy is summarised in **Figure 4**. The oldest sediments penetrated within the Endurance area are those deposited during the mid to late Carboniferous, unconformably overlain by a thick sequence of Permian, Triassic and early Jurassic sediments. A major unconformity separates the Jurassic from the Cretaceous to Cenozoic stratigraphy.

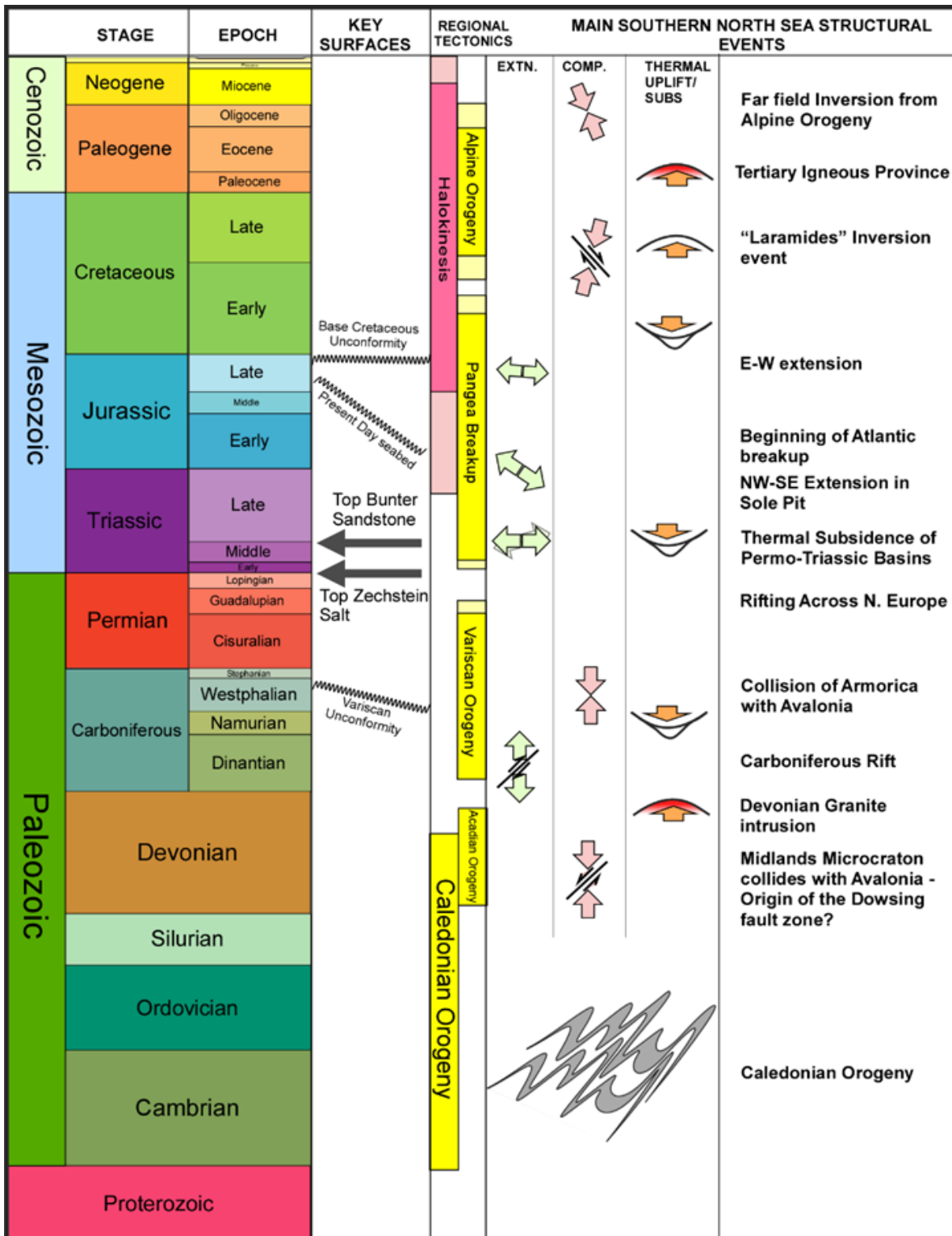


Figure 3 - Regional tectonostratigraphy of the Southern North Sea.

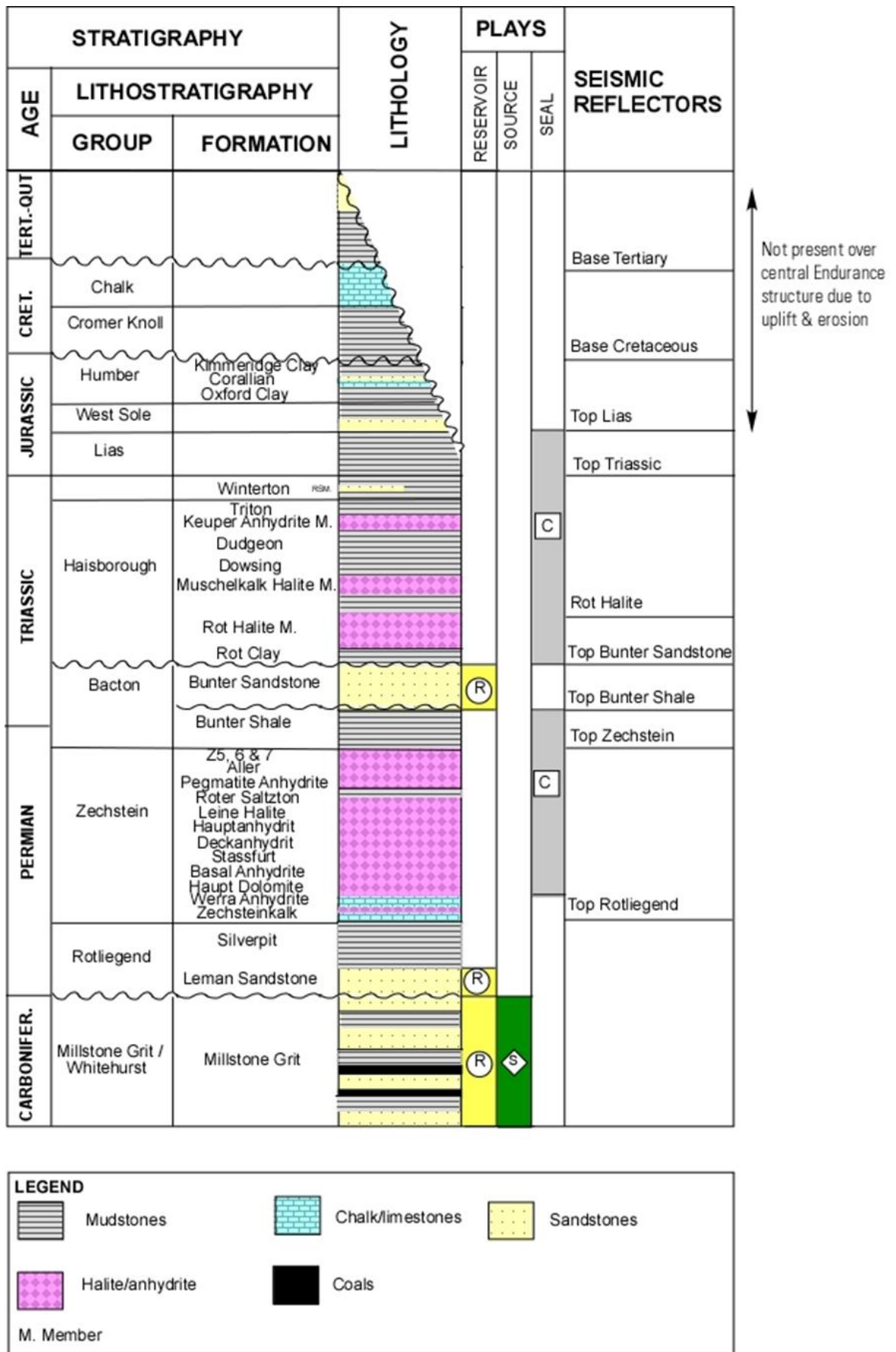


Figure 4 - Stratigraphic column for the Southern North Sea.

1.3.1.1 Ordovician to Carboniferous

Much of the structural fabric originates from the Caledonian and Variscan plate tectonic cycles during the Palaeozoic (Underhill, 2003). The Ordovician to Devonian Caledonian Orogeny influenced the development of NW–SE striking structures aligned with the northeastern boundary of the Midlands Microcraton during the Devonian (e.g. the Dowsing Fault Zone) (Guterch et al., 2010). Lithospheric extension and rifting commenced during the late Devonian to early Carboniferous, with active fault-bounded half grabens and tilted fault blocks developed in the Southern North Sea area, following the NW–SE trends of the older Caledonian basement (Coward et al., 2003; Moscariello, 2003). By the Late Carboniferous, the Southern North Sea area had transitioned to humid equatorial conditions and was an established deltaic province, characterised by deltaic to fluvio-lacustrine deposits with numerous coal layers (Underhill, 2003; Kombrink et al., 2010). Subsequent compression associated with the Variscan Orogeny resulted in fault reactivation, folding, uplift and erosion of the Carboniferous strata, with progressively younger Carboniferous-age rocks sub-cropping from west to east beneath the Variscan Unconformity (Moscariello, 2003; Grant et al., 2018).

1.3.1.2 Permian

Subsidence in the early Permian, in response to post-orogenic collapse and rifting at the end of the Variscan Orogeny, led to the development of the intracratonic Southern Permian Basin. This was an extensive basin which extended from the UK Southern North Sea eastwards as far as Poland (Underhill, 2003; Grant et al., 2018). Syn-sedimentary rifting occurred during the Permian, influenced by the NW–SE basement fault trends, which continued to be reactivated repeatedly during the Mesozoic and Cenozoic.

The ongoing plate tectonic movements meant that by the time the Southern Permian Basin was initiated it had drifted northwards of the equator to within the northern hemisphere desert belt (Glennie, 1997). An arid climate prevailed and the Permian Rötliengend Group deposition was within an entirely land-locked basin, with terminal playa and saline lakes developed in the central, deepest parts of the basin. Within the Southern North Sea area, the Rötliengend Group is represented by two key formations: the Lemn Sandstone Formation and the Silverpit Formation. The Lemn Sandstone Formation consists of cross-bedded, dune sandstones deposited within an aeolian desert environment, which laterally grade northwards into the Silverpit Formation, composed of mudstones and interbedded evaporites deposited within a playa lake environment (Gast et al., 2010; Underhill, 2003).

The Southern Permian Basin was flooded by marine waters during the late Permian. The Zechstein Group depositional environment reflects cycles of marine incursions which subsequently increased in salinity and progressively evaporated, leading to cyclic deposition of marine carbonates and mudstones followed by widespread evaporite deposits (Glennie, 1997; Underhill, 2003).

1.3.1.3 Triassic

The active basin extension in the Southern North Sea area waned through the late Permian and was succeeded by a phase of thermal subsidence, a period of tectonic quiescence which continued through the Triassic to Early Jurassic times (Underhill, 2003; Grant et al., 2018). Semi-arid continental conditions also returned at the end of the Permian. Ephemeral fluvial systems drained northwards off the Variscan fold belt and the Triassic Bacton Group sediments (Bunter Shale Formation and Bunter Sandstone Formation) were deposited in predominantly fluvial, lacustrine and playa lake environments, which were subject to aeolian reworking (Bachmann et al., 2010; Geluk et al., 2018). In the mid Triassic, episodic marine incursions into partially restricted basins under dry climatic conditions resulted in the deposition of marine (and subordinate lacustrine) evaporites, mudstones and limestones of the lower Haisborough Group (Geluk et al., 2018; Moscariello, 2003). In the late Triassic, more non-marine conditions returned, with deposition of clastics, evaporites and carbonates in ephemeral lake and fluvial systems (upper Haisborough Group). At the end of the Triassic (Penarth Group), there was a marine transgression and the depositional environments transitioned from non-marine, through paralic systems to marine conditions by the early Jurassic (Bachmann et al., 2018).

Subsidence in the Triassic–Jurassic was controlled by continued extension on the Dowsing Fault Zone, but sediment distribution was increasingly affected by salt tectonics, whereby the Zechstein Salt that had been deposited during the Late Permian formed into salt swells in response to the developing sedimentary load (Stewart & Coward, 1995; Pharaoh et al., 2010).

1.3.1.4 Jurassic to Early Cretaceous

Global sea level rise and flooding in the early Jurassic created a shallow epicontinental basin into which shallow, open-marine, fine-grained mudstones of the Lias Group were deposited (Lott et al., 2010). In the mid Jurassic, thermal doming and uplift in the region of the North Sea Rift triple junction to the north of the Southern North Sea led to considerable erosion and removal of much of the Mesozoic section (Stewart & Coward, 1995; Pharaoh et al., 2010). The subsequent collapse of the thermal dome culminated in the extensional tectonics of the North Sea Rift during the Late Jurassic to Early Cretaceous, which was expressed as transtensional subsidence in NW-SE trending Sole Pit Basin, whilst rift flank uplift and erosion took place to the northeast, resulting in a combined complex of unconformities known as the Base Cretaceous Unconformity (Stewart & Coward, 1995; Pharaoh et al., 2010; Grant et al., 2018). The remainder of the Jurassic section after the Lias Group is absent in the area of interest due to the erosion associated with the Base Cretaceous Unconformity.

1.3.1.5 Late Cretaceous to Cenozoic

Open-marine depositional environments continued throughout the Cretaceous, with the deposition of shallow-marine argillaceous sediments of the Cromer Group in the Lower Cretaceous, followed by a thick sequence of chert-rich limestones, chalks and marls of the Chalk Group in the Upper Cretaceous (Moscariello, 2003). Post-rift thermal subsidence was established over the Southern North Sea area by the Late Cretaceous. Towards the end of the

Late Cretaceous and throughout the Early Cenozoic, there was widespread basin uplift and several pulses of structural inversion related to the opening of the Atlantic Ocean and Alpine collision in Europe (Pharaoh et al., 2010; Grant et al., 2018). Within the Silverpit Basin, the structure is dominated by NW-trending Zechstein Salt pillows and walls, folding the post-Permian sequence into a series of NW-SE trending anticlines and synclines. Widespread halokinesis of the Zechstein salts was triggered by the Cenozoic inversion and reactivation of basement faults under a dextral transpressional regime (Pharaoh et al., 2010; Conway & Valvatne, 2003; Moscariello, 2003). The final phase of inversion was in the Oligocene–Miocene, after which time thermal subsidence resumed and the remainder of the Cenozoic is characterised by marine and glacio-marine argillaceous sandstones, siltstones and clays (O'Mara et al., 2003; Moscariello, 2003).

1.4 Exploration and Appraisal History

Exploration for hydrocarbons first commenced in the Southern North Sea in the 1960s, targeting possible gas at the Triassic Bunter Sandstone 4-way structural closures. This led to the Endurance reservoir being discovered by well 43/21-1, drilled by Mobil in 1970 at the crest of Endurance, which found very saline brine. A suite of conventional logs was run, and the well was abandoned. A second well was drilled by BP in 1990, 42/25-1, targeting the deeper stratigraphy, and confirmed water-bearing at the Triassic Bunter Sandstone interval. Well 42/25d-3 was drilled by National Grid Carbon in 2013 as an appraisal well for the White Rose CO₂ storage project, gathering valuable data including 190m of core.

1.5 Storage Site and Storage Complex

The proposed CO₂ injection reservoir is the Triassic-age Bunter Sandstone Formation within the structural closure of the Endurance anticline (Storage Site). Containment is provided by the overlying Röt Clay and Röt Halite (base Haisborough Group) as primary seals, plus secondary seals within the remainder of the Haisborough Group, Penarth Group and Early Jurassic. The Storage Complex is defined as the Bunter Sandstone Formation reservoir and overlying Röt Clay, Röt Halite and other seals up to the Jurassic Lias Group, within the structural closure of the Endurance anticline and extending southeast to include the 'outcrop' (a region where the Bunter Sandstone Formation has been folded up to outcrop at seabed due to an underlying Zechstein salt diapir). The Storage Site and Storage Complex are shown in **Figure 5** and the key characteristics are summarised in **Table 1**.

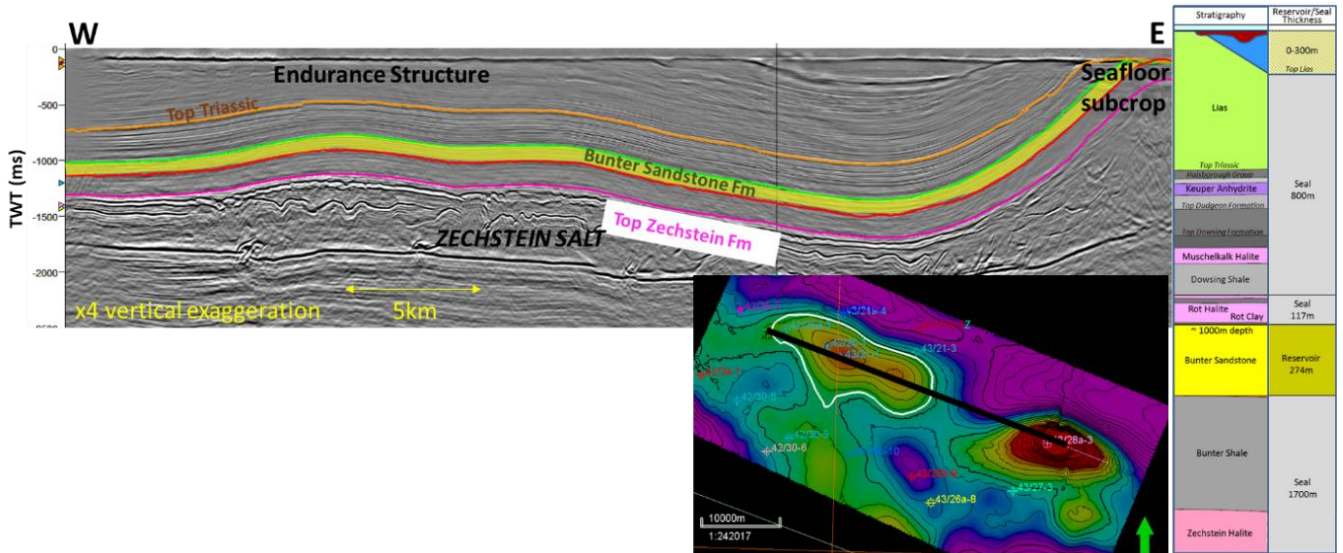


Figure 5 - Endurance storage complex.

Table 1 - Summary of key characteristics of the Endurance CO2 store.

| Parameter | | Units | Value / Comment |
|-----------|----------------------|--------|-------------------------------|
| Reservoir | Formation | | Bunter Sandstone Formation |
| | Age | | Triassic (Bacton Group) |
| | Type | | Fluvial-aeolian sandstones |
| | Average thickness | m | 275 |
| | Average net to gross | % | 94 |
| | Average porosity | % | 22.5 |
| | Average permeability | mD | 300 |
| Trap | Average salinity | ppm | 250,000 |
| | Type | | Four-way dip closed anticline |
| | Depth to crest | mTVDSS | 1000 |
| | Spill point | mTVDSS | 1450 |

Primary Store Geological Model and Report

| | | | |
|-------------------------|------------------------------------|--------|-----------------------------------------|
| | Area | km2 | 140 |
| Seal | Formation | | Röt Clay and Röt Halite |
| | Age | | Triassic (Haisborough Group) |
| | Type | | Playa lake mudstones & evaporites |
| | Thickness | m | 110: Röt Clay 10 + Röt Halite 100 |
| Reservoir conditions | Datum depth | mTVDSS | 1300 |
| | Initial pressure at datum depth | Psi | 2030 |
| | Temperature at datum depth | °C | 57 |

2.0 Reservoir Characterisation: Sedimentology of the Bunter Sandstone

2.1 Previous work

There is a wealth of sedimentological description of the Bunter Sandstone reservoir that has previously been conducted on Endurance during earlier phases of work associated with the White Rose project. Leppard (2011) studied core acquired from ten regional wells in the Southern North Sea, and Blackburn (2012) and Blackburn & Robertson (2014) described the cores from the two wells on the Endurance structure (42/25-1 and 42/25d-3, respectively). Cuttings from well 43/28a-3 located on the outcrop, which penetrates Bunter Sandstone in the top ~400m of the well, were also described by Blackburn (2014).

Those studies described the Bunter Sandstone as deposited in a semi-arid, land-locked basin with fluvial systems that terminated in playa lake, playa margin, aeolian dune and sabkha settings. Sedimentation rates were low (100m/3Ma) with considerable reworking and recycling via fluvial and aeolian processes. As a result, it was interpreted that irrespective of the final mode of deposition, many of these sediments have similar reservoir characteristics. Based on this understanding, reservoir modelling for the White Rose project was conducted using an electrofacies approach and relatively short variograms of one length.

2.2 Lithotype Core Study

A review of the previous work identified a gap in this description with respect to the link between depositional facies and reservoir properties and the impact of baffle/barrier lithotypes on heterogeneity within the static model. This resulted in a supplementary study of the 42/25d-3 core being completed for this project, a lithotyping exercise with a focus on identifying potential baffle/barrier lithotypes and understanding their deposition to underpin their distribution within the static model.

A lithotype scheme was established and used to describe ~130m of well 42/25d-3 sandstone core (cores 2,3 & 4). It was also used at a high level to describe differences between wells 42/25d-3 and the 42/25-1 and cores from the Hewett field to provide a brief comparison of depositional settings.

2.3 Core Overview

Cores 2, 3 and 4 from well 42/25d-3 are reddish sandstone with very rare silt and mud layers, dominated by cross-bedded, laminated and rippled sands. A smear or salt-crust is present on the surface of the core, particularly in the uppermost sections (core 2). The sands are very occasionally carbonate cemented. Large-scale erosional boundaries or potential stratigraphic surfaces are rare to absent, and upon first observation the cores appear relatively homogeneous, although on further examination, lithotyping trends and packages are apparent.

Grain size is generally consistent, around very fine upper, and silt drapes on sedimentary structures are common. While heterogeneity at the log-scale is relatively low, at the core- to core-plug-scale it is likely to be quite high.

An attempt was made to divide the unit up into packages, and from there into vertical trends. The salt-crust was removed from areas where it was obscuring the rock beneath and lithotyping was documented on the core photographs, which were later digitized. There is significant uncertainty associated with this interpretation and numerous alternatives exist which it was important to capture model.

2.4 Lithotypes Guide

The lithotypes and sub-lithotypes as defined for the study are shown in **Table 2**.

Table 2 - Lithotypes and sub-lithotype scheme developed for cores 2, 3 and 4 of the Bunter Sandstone Formation from well 42/25d-3.

| Lithotype | Sub-type | Brief Description | Indicative depositional setting | Key Photos |
|-----------|----------|-----------------------------------------------------------------------------------------------------------------|---------------------------------|---------------------------------------------------------------------------------------|
| SM | SM | Massive sands. No clear lamination or sedimentary structures on the cm-scale or greater. | None | |
| SL | SL | Laminated sands on the mm-cm scale. Defined by either grain size alternations or silty-muddy drapes on laminae. | None | |
| | SLtl | Thinly laminated sand, almost pinstripe in character. Extremely regular in appearance on the 10s cm scale. | Possible aeolian |  |

| | | | | |
|----|------|-----------------------------------------------------------------------------------------------------------------------------------------------------------------------------------|---------|---------------------------------------------------------------------------------------|
| SD | SD | Soft sediment deformation – slumps and slides. Includes dewatering features. | Fluvial |  |
| SR | SR | Rippled sand without climbing. Ripples defined by silty-muddy drapes | Fluvial |  |
| | SRcl | Climbing ripples, units often on the 10s cm scale. | Fluvial |  |
| | SRcr | 'Crinkly' ripples (may be described as adhesion ripples, when taken forward to process description). Disturbed regular laminae with 5mm-scale relief, without clear organisation. | Aeolian |  |
| | SRd | Diffuse, subtle rippled units, defined only by | Unknown | |

| | | | | |
|----|------|------------------------------------------------------------------------------------------------------------------------------------------------------------------------------------------------------------|------------------|--------------------------------------------------------------------------------------|
| | | sand grain size and potentially cementation, rather than by silty-muddy drapes. | | |
| SX | SXt | Trough cross bedding at the 10s of cm scale. | Fluvial |  |
| | SXp | Planar cross-bedding. | None | |
| | SXps | Planar cross-bedding that can be seen to steepen up at the metre scale, from effectively flat lying, where it may be mistaken for SL lithotype, to ~40-degree dip angles. Often occurs in repeated cycles. | Possible aeolian | |
| | SXI | Low-angle cross lamination with very subtle terminations. May at a first glance be mistaken for SLtl lithotype. | Unknown | |

| | | | | |
|-----|-----|----------------------------------------------------------------------------------------------------------------------------------------------------------------------------------------------------------------------------------------------------------------------|--------------------|--------------------------------------------------------------------------------------|
| SLT | SLT | Homogenous, cm-scale silt layers, often displaying sand-filled mud cracks and very occasionally potential insect burrows. | Low-energy setting |  |
| H | H | Interbedded thin silty layers, thin rippled or laminated sands, and extensive platy mud clasts that 'almost' form layers (these appear to be highly locally sourced and are likely the remnants of thin dessicated mud layers). Heterolithic on the 10s of cm scale. | Low-energy setting |  |
| M | M | True clayey muds, mostly laminated. | Low-energy setting | |

Additional 'flags' were also developed and manually identified on core photos. These relate to sedimentological features that were useful in developing the understanding particularly of potential baffles. These were as shown in **Table 3** below.

Table 3 - Flags and sub-flags used in lithotyping scheme developed for cores 2, 3 and 4 of the Bunter Sandstone Formation from well 42/25d-3.

| Flag | Sub-type | Brief Description | Key Photos |
|--------|----------|-------------------------------------------------------------------------------------------------------------------------------------------------------------------------------------------------------------|---------------------------------------------------------------------------------------|
| SFMC | | Sand-filled mud cracks; likely dessication cracks providing vertical pathways across silty layers and indicating short-term exposure and drying out |  |
| MC | MCR | Mudclast rounded – larger size, likely further transported in reworking. All mudclasts appear to be sourced from the ‘silty’ layers, no clear extraformational clasts |  |
| | MCP | Mudclast platy – generally finer scale mudclasts, often defining sedimentary structures. In some instances, may also be extremely (cm- to mm-scale) locally reworked from thin silty layers with mudclasts. |  |
| Cement | | Cemented layers – white (reduced?) in colour, much harder, sometimes patchy and sometimes more extensive |  |

| | | | |
|------------------|--|------------------------------------------------------------------------------------------------------------|-------------------------------------------------------------------------------------|
| <p>Blue line</p> | | <p>Indicates the location of an erosional base, including within lithotypes. May contain mudclast lag.</p> |  |
|------------------|--|------------------------------------------------------------------------------------------------------------|-------------------------------------------------------------------------------------|

2.5 Depositional Environment Interpretation

Potential packages were defined based on shifts in dominant lithotype, lithotype assemblages and erosional bases. In some cases, these matched those defined by Blackbourn & Robertson (2014), and in others not.

The cores reflect an overall fluvial-aeolian type setting, with highly reworked depositional elements. While many diagnostic-setting sedimentary structures occur (e.g. climbing ripples and trough crossbedding for fluvial, steepening upward cross-sets and adhesion ripples for aeolian), there are few to no clearly observable depositional elements. Rather, the overall effect is of an amalgam of remnant dunes, small-scale stream channels, splays and rare interfluves in a highly reworked, low accommodation space setting. There was no organic matter seen anywhere in the core, and very rare bioturbation (insect burrows) indicating the environment was very barren and extremely hostile to life.

Due to the low accommodation space and extensive reworking, it is unlikely that any one depositional element is completely preserved, and therefore dimensional width/thickness relationships are unlikely to apply. However, it is clear from the decimetre-scale bed boundaries common throughout the section that any individual bedset is unlikely to extend more than ten metres laterally, based on analogy with other known sedimentary formations (e.g. Tunbridge Wells Sands Unit of the Weald Basin).

2.6 Analogues and Implications for Modelling

Modern and ancient analogues were reviewed to understand the depositional extents of the sedimentary facies observed in core at 42/25d-3. Modern analogues were identified in places such as Western Iran, Taklimakan Desert in China, Chott el Djerid in Tunisia, the Sistran Basin between Eastern Iran and Afghanistan and Khongoryn Els in Mongolia. An example of Khongoryn Els, in the extreme south of the Gobi Desert, Mongolia, is shown in **Figure 6**. Ancient analogues were provided by the existing Bunter Sandstone gas fields within the Southern North Sea and outcrop of analogous formations within onshore UK.



Figure 6 – Images from Khongoryn Els, Mongolia, showing small-scale features associated with small ephemeral lake systems, a modern analogue for the Bunter Sandstone Formation depositional environment.

Bunter Sandstone is the reservoir formation for eight fields in the UK Southern North Sea. A review of production performance from Bunter Sandstone gas reservoirs was conducted during the previous White Rose project on Endurance. In summary these studies concluded that depletion characteristics of Bunter Sandstone gas accumulations during production reflects a range of diagenetic and depositional controls on reservoir performance. In the east, the Caister and Hunter fields suggest that internal barriers to vertical flow are present where finer grained, more distal units are preserved and are able to support significant pressure differentials. To the north, the Esmond complex of fields in Bunter Sandstone reservoirs are more proximal to Endurance and data suggests fewer vertical barriers from pressure measurements and production data compared with Caister B field. An analysis of production and post-production pressure data has been modelled (see Dynamic Model KKD).

Onshore ancient analogues include the Cretaceous fluvial sandstones of the Weald Basin (Tunbridge Wells Sands unit). Whilst not a direct analogue, this may help as an illustrative aid. The high net sands of the Southern Sandstone consist dominantly of decimetre-scale fluvial cross-beds with some ripples. While the aeolian elements are absent here, the lateral continuity of any one set of cross-beds (around 1 – 3m) and the lack of any key bed-bounding surfaces to control the overall deposition may be a useful visual aid to demonstrate variability in the field.

Such modern and ancient analogues demonstrate the rapidly changing and extensively reworked nature of the depositional setting. The changeability of the lithotypes on the sub-metre scale and the lack of clear distinction between lithofacies determined that object-based modelling was not appropriate within the static model.

2.7 Surfaces/transmissibility Barriers

Potential baffles/barriers identified from lithotypes and lithotype flags for inclusion in static modelling are discussed below.

2.7.1 Cements

There were two types of cement identified in core: a 'crumbly' cement/crust at the top of the core, and a more conventional, possible patchy cement throughout.

2.7.1.1 Crumbly Cement/crust

This correlated heavily with the occurrence of a thick, salty encrustation on the surface of the core – it is this which required cleaning and obscures sedimentary structures in the original photos. It occurred dominantly within Core 2 and was associated with a crumbly texture increasing in intensity towards a surface at approximately 1409 mMD.

2.7.1.2 Patchy Bleached Cement

This cement is more conventional, and integrating XRD data, appears likely to be localised carbonate cement. The cement was flagged as above in **Table 3** in order to examine its relationship to reservoir quality and petrography.

The cemented units are patchy, usually extensive across the core. They are generally of the order of 10cm in thickness, although there are some occurrences at the m-scale. They appear pale greenish in colour, in contrast to the dark red of the rest of the formation so are quite clear on photographs. They are harder than the rest of the formation and are clearly suppressed in permeability. Generally, they occur in association with minor surfaces such as channel bases or tops, sometimes locally associated with mud clasts.

A single instance of this cement, at around 1420 mMD, covered several metres continuously in the core and may be associated with a more regional surface. In the petrographic data provided, it is apparent that this section is associated with abundant ooids within the clastic sediment. Although it cannot be ruled out that these carbonate ooids formed depositionally, it is more likely that these ooids are derived from the underlying Triassic interval and have been reworked effectively as grains of sand.

2.7.1.3 Cemented Surfaces

The small-scale calcite cemented, and bleached horizons generally seem to be associated with either the bases or tops of channel cuts, and are therefore likely to have extents that correspond (at the maximum) to the dimensions of the channels, sub-100m grid cell based on analogue depositional settings.

The cemented interval at the multi-m scale, associated with reworked ooids, discussed above may also represent an extensive surface. If these ooids are derived from a local hinterland their deposition may occur across the basin, and indeed in the other core examined (42/25-1) at an approximately similar position through the interval a similar pale horizon with increased carbonate material occurs. This can also be seen in the uncored well on structure 43/21-1.

2.7.2 Heterolithics

2.7.2.1 Silty Mud-crack Surfaces

The most likely extensive baffles in the core (there may be more in other areas of the field or unpenetrated zones) are cm to ~10 cm silty layers that often form half-metre scale heterolithic units. These silty layers include rare bioturbation (likely insect traces), common sand filled mud cracks and are associated with small-scale rippled sands. They also occur with massive sands with flat-lying platy mudclasts, which can be assumed to be slightly remobilised thin silt layers, very locally reworked by a subsequent ripple-flow. There is no rooting or soil development.

- These are the most likely surfaces to be extensive. The lateral extent is dependent on their interpretation:
- Interfluvial settings - may be extensive if a number of point sources of sediment are assumed
- Margins of a playa lake – more extensive than interfluvial

Stratigraphic surface associated with shifts in climate or sediment supply. As this time period apparently bracketed by the Bunter Sandstone is on the order of a few million years, it is possible that in this period a number of climatic cycles may have occurred, and that these have sedimentological expressions such as a shift in facies proportions or a shut-off of sediment supply points

It is important to state clearly that these beds do not represent true lacustrine facies; they do not display any characteristics of prolonged sub-lacustrine deposition. They are simply lower-energy sedimentary structures that show some submerged/dessicated features that are more likely to occur closer to a body of water.

2.8 Potential Facies Types

Figure 7 is a summary diagram highlighting alternative models for reservoir connectivity. These images are scaled to a single grid cell in the static model and demonstrate the ‘melange’ nature of the sedimentary structure observed in core, as well as the potential extension of the heterolithic surfaces.

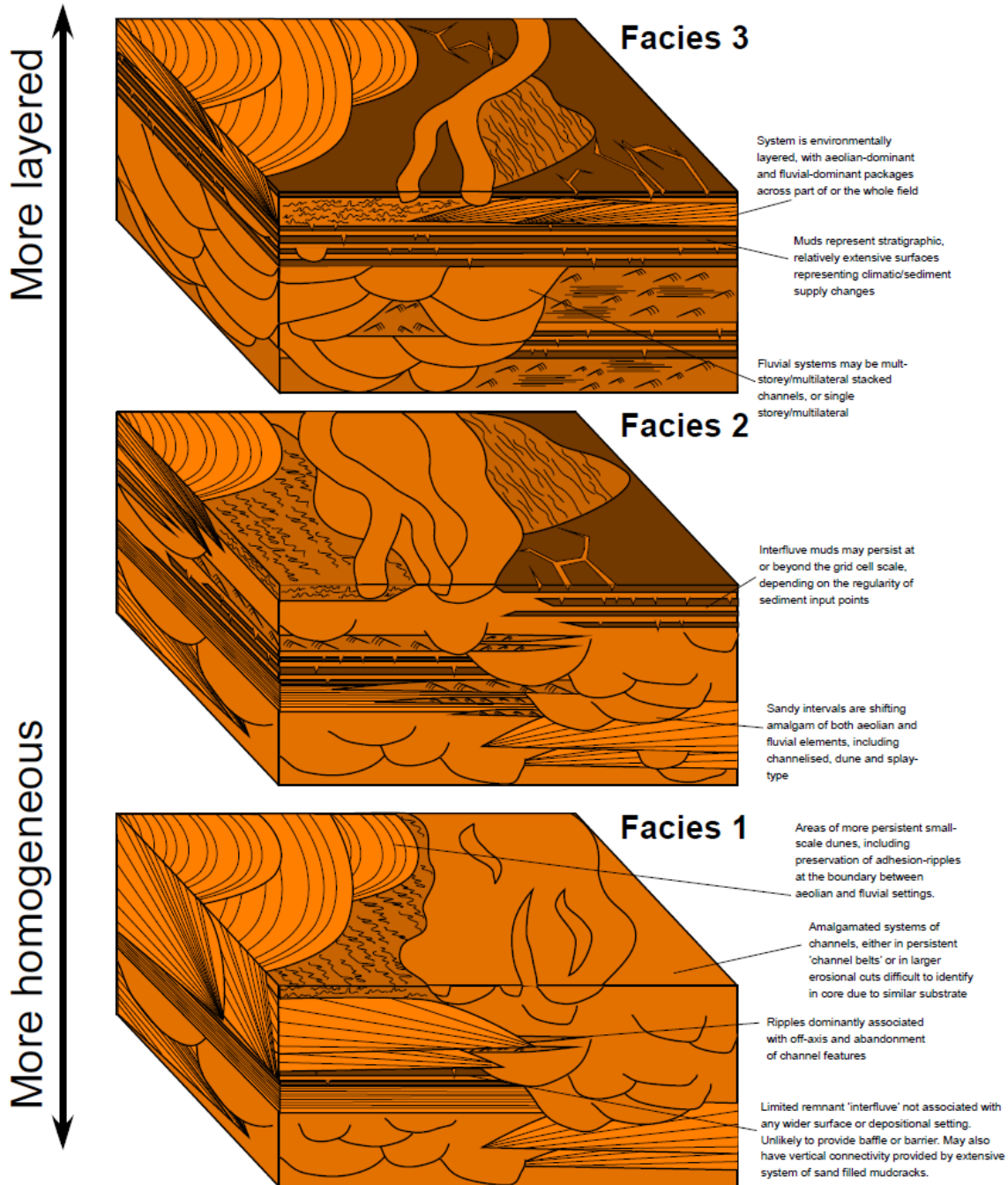


Figure 7 - Summary diagram highlighting alternative models for reservoir connectivity.

2.9 Lithotype Rock Properties Variation

Good sands of the lithotypes identified as aeolian, fluvial and mixed have broadly similar porosity-permeability characteristics (**Figure 8**). Potential baffle/barrier lithotypes and flags show decreased values (**Figure 9**). However, some core plugs at the low end of the good sand range still show reasonable values, particularly in the horizontal direction. Reasons for this may be inferred from the sedimentological descriptions above. For example, heterolithic lithotype sections include sand-filled mud cracks which are likely dessication cracks but contain vertical pathways across silty layers. Heterolithic and low-energy facies correlate well with electrofacies derived from petrophysics.

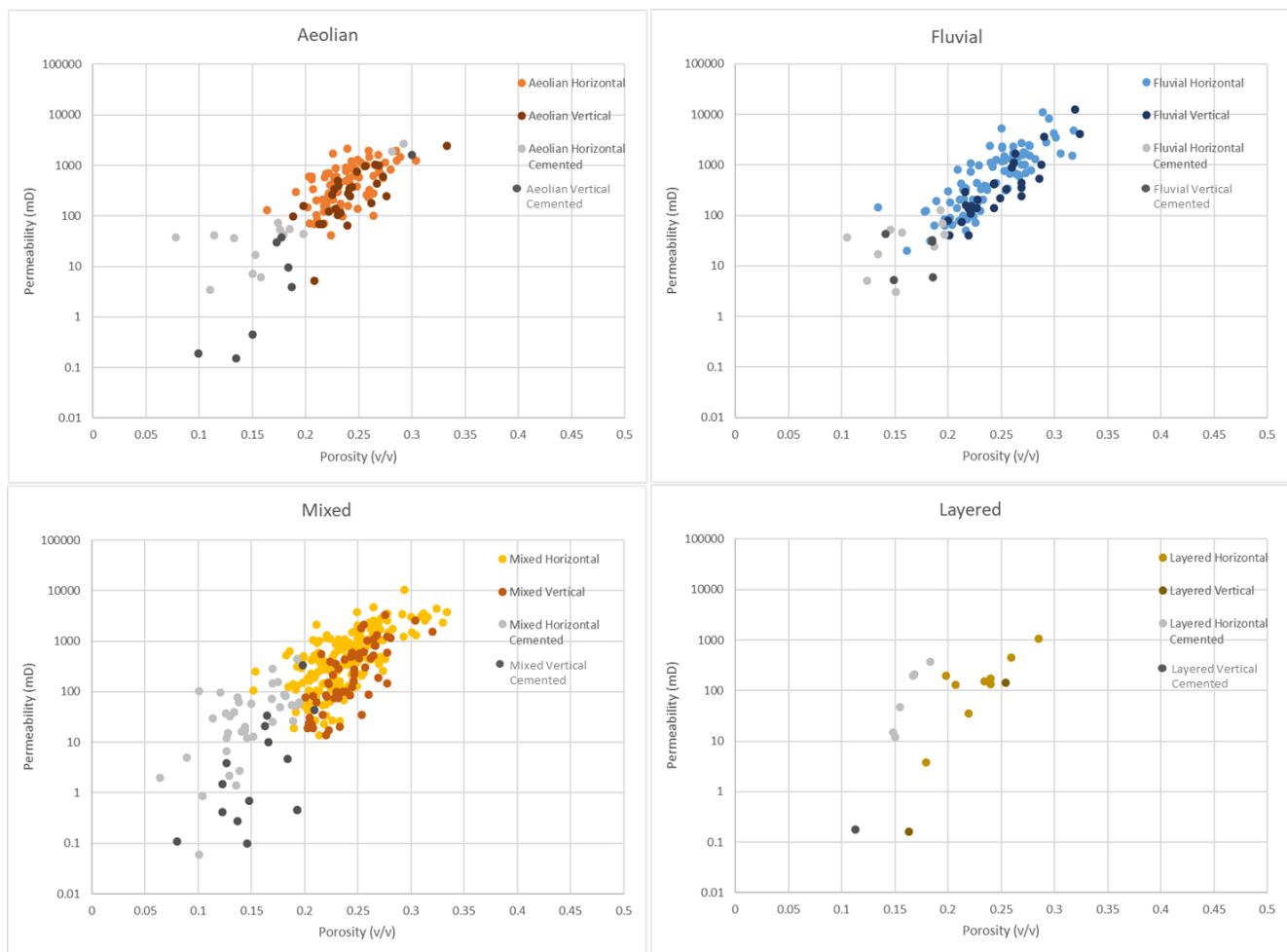


Figure 8 - RCA porosity and permeability test data (non-overburden corrected) cross-plotted for the different facies identified by particular lithotypes. Datapoints flagged as cemented from core interpretation or potentially cemented are coloured grey to highlight lower properties. Light and dark colours are used to denote horizontal plug data from vertical respectively.

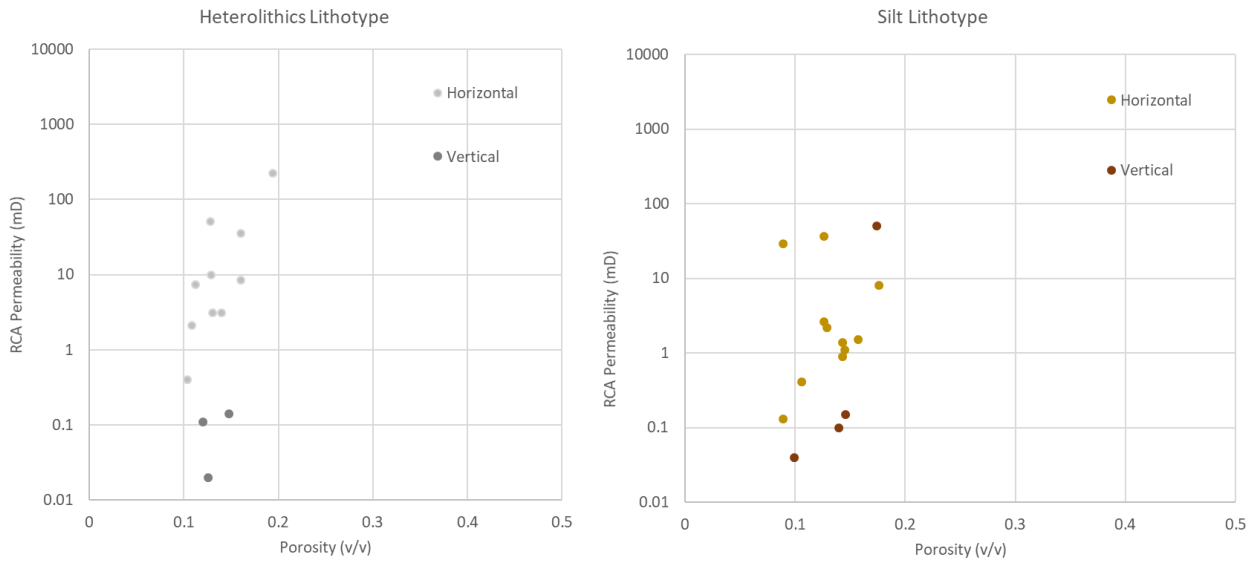


Figure 9 - RCA porosity and permeability test data (non-overburden corrected) cross-plotted for potential baffle/barrier lithotypes. Light and dark colours are used to denote horizontal plug data from vertical respectively.

3.0 Petrophysical Model

A petrophysical model has been created for the evaluation of the saline water bearing Bunter Sandstone at the Endurance CO2 store. Note that the model is calibrated at Endurance and whilst still applicable to the Bunter Sandstone elsewhere in the basin, it is recommended to check the underlying geology and fluids are still comparable when using these parameters away from Endurance.

3.1 Data Inventory

Core data and wireline log data had been acquired by the three wells drilled in the Endurance structure. The data available for this study is summarised in **Table 4**. Well 42/25d-3, which had been drilled as an appraisal well for the White Rose project, provides the most comprehensive dataset.

Table 4 - Core and wireline log data available over Endurance structure.

| Data | | 42/25-1 | 42/25d-3 | 43/21-1 |
|---------------------------------------------|---------------|-------------------------------------------------|---------------------------------------------------------------------------------------------------------------------------------------------------------------------------------------------|---------|
| Core | No. / Length | 1 core: 18 m | 4 cores: 192.51 m in total (631.6 ft) | - |
| | Core analysis | Porosity, permeability, grain density (ambient) | Porosity (ambient & stressed), permeability (air/Klinkenberg/brine, ambient & stressed), grain density, XRD, MICP, petrography, relative permeability | - |
| Wireline logs | Basic* | Yes | Yes | Yes |
| | Advanced | Formation pressures | Formation pressures Fluid samples Mini-frac Vertical interference test (VIT) Image logs: dual OBMI – UBI (although considered poor quality) Nuclear magnetic resonance (NMR) | - |
| * Gamma ray, resistivity, density and sonic | | | | |

3.1.1 Volume of Clay (VCL)

An initial Vcl was calculated using the Gamma Ray (GR) values observed in the well. The sand (clean) GR value was taken as the minimum of the Gamma Ray values over the Bunter Sandstone formation. The clay (shale) GR value was taken as the maximum of the Gamma Ray values over the Röt Clay formation.

A simple linear calculation is then used to provide the initial Vcl estimate:

$$Vcl_{initial} = \frac{GR_{Measured} - GR_{Sand}}{GR_{Clay} - GR_{Sand}}$$

The XRD data from well 42/25d-13 was then used to calibrate the initial Vcl calculation to produce the final Vcl calculation shown below:

$$Vcl_{final} = 0.4476421 \times Vcl_{initial} - 0.02305182$$

3.1.2 Porosity

The primary method of calculating porosity is using a density log. A simple density porosity is calculated, using a matrix density of 2.66 g/cc and a fluid density of 1.05 g/cc. The grain density value is taken from the core analysis data and the fluid density value is a result of the calibration of the density log to core. Density porosity was calculated in the 42/2511, 42/25d-3 and 43/21-1 wells using the formular below:

$$PHIT_D = \frac{\rho_{matrix} - \rho_{measured}}{\rho_{matrix} - \rho_{fluid}}$$

A sonic porosity was also calculated using the Raymer–Hunt–Gardner equation with a matrix slowness of 55 us/ft and a fluid slowness of 189 us/ft (these values are chartbook derived). This is used for the primary porosity calculation in well 43/27-3, which is outside of the main Endurance structure:

$$PHIT_S = 1 - \frac{DT_{Matrix}}{2 \times DT_{Fluid}} - \sqrt{\left(\frac{DT_{Matrix}}{2 \times DT_{Fluid}}\right)^2 - \frac{DT_{Matrix}}{DT_{Fluid}} + \frac{DT_{Matrix}}{DT_{Measured}}}$$

The wells in the aquifer generally have a sparse dataset over the Bunter Sandstone. Consequently, a resistivity-based porosity was used in these wells. This is calculated by using an Archie water saturation calculation, assuming Sw=1, a=1 and n=1:

$$PHIT_R = \left(\frac{R_w}{R_t}\right)^{\frac{1}{m}}$$

To derive the remaining properties a pickett plot between core porosity and deep resistivity from well 42/25d-3 is used. This results in an m value of 1.776 and an Rw of 0.0454 ohm.m (@20°C).

3.1.3 Permeability

Log permeability is calculated using a porosity/permeability relationship derived from the core data collected in the 42/25d-3 and 42/25-1 wells. At the time this petrophysical model was initially created no overburden corrected core data was available. Consequently an overburden correction for permeability was created using regional analogue data, using a method outlined in the literature (Prediction of brine permeabilities at overburden pressures from routine core analysis data by M.K.Brooks and I.J.Evans). Overburden corrected core porosity was assumed to be 0.94 x CPOR (atmospheric pressure), this assumption was taken from previous work and was not able to be tested for validity.

Overburden corrected porosity was then plotted against overburden corrected permeability and a single regression was calculated (**Figure 10**). This regression was then used to predict brine permeability from porosity.

$$\text{Brine permeability (2600Psi)} = 10^{(4.8773 \times \log_{10}(\text{PHIT}) + 5.727295)}$$

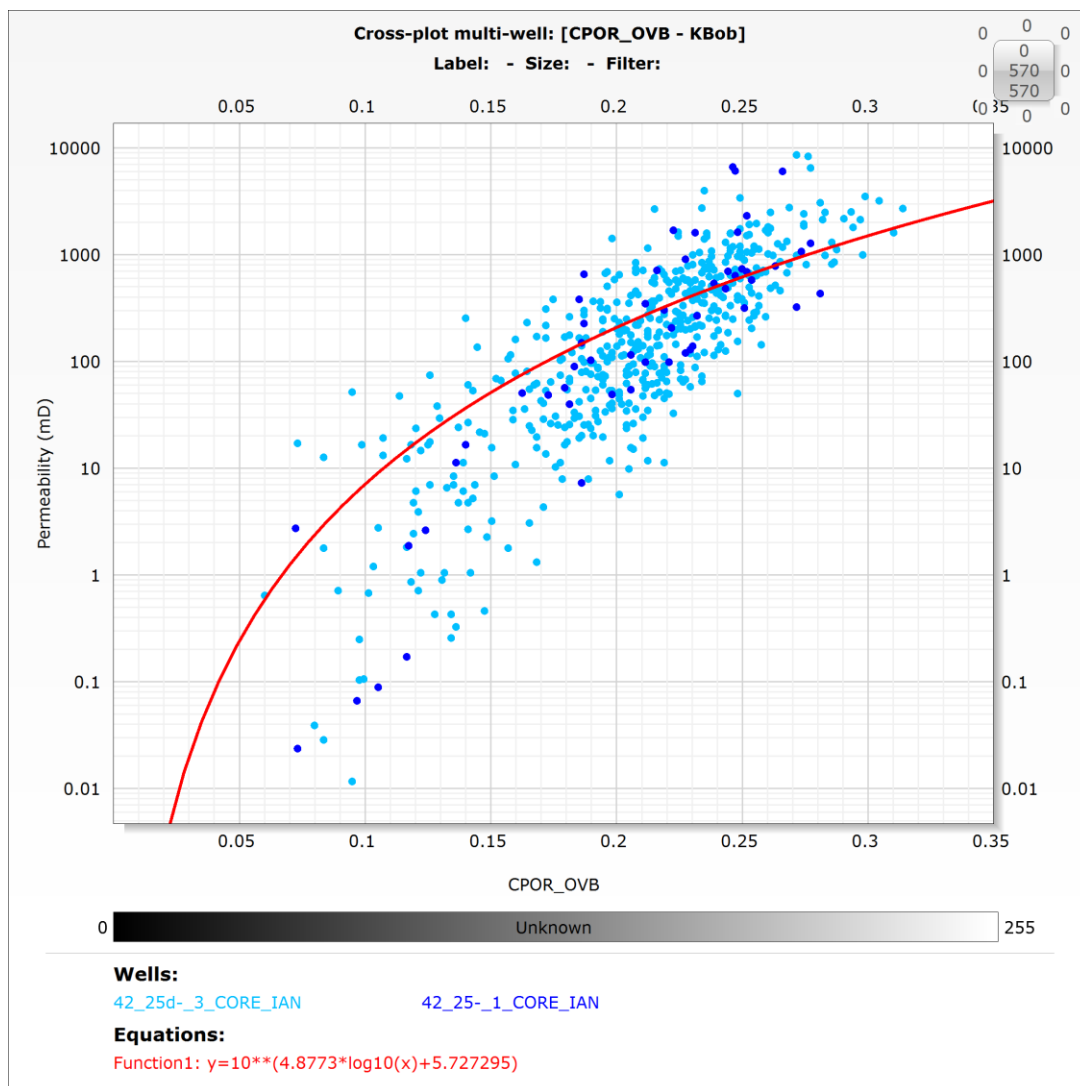


Figure 10 - Overburden corrected porosity versus brine permeability (overburden corrected). Red line is the Porosity (PHIT)/Permeability transform.

In earlier versions of the static model this was then adjusted to fit with dynamic test data from well 42/25d-3. This is detailed in the later sections on static modelling (section 0). When ‘at stress data’ was obtained, the reason for this adjustment was found to be the overburden correction which has been corrected in later versions of the model.

3.1.4 Net Reservoir

Net reservoir is defined as having volume of clay (VCL) <0.2 and porosity (PHIT) > 0.05. Due to the lack of dynamic data available these cut-offs are not well constrained and have a significant associated uncertainty.

3.1.5 Property Summary

Average properties are shown in **Table 5** for the three wells on the main Endurance structure. Please note that 42/25-1 is a partial penetration and does not sample the entire Bunter Sandstone.

Table 5 - Endurance wells petrophysical property summaries (reference to TVDSS).

| Well | Top (m) | Bottom (m) | Gross (m) | Net (m) | Net to Gross (m/m) | PHIT (v/v) | Brine Perm (mD) |
|----------|---------|------------|-----------|---------|--------------------|------------|-----------------|
| 42_25-1 | 1080.1 | 1152.2 | 72.1 | 71.8 | 0.995 | 0.228 | 535.8 |
| 42_25d-3 | 1368.7 | 1591.7 | 223.0 | 215.6 | 0.967 | 0.203 | 378.7 |
| 43_21-1 | 1023.0 | 1269.0 | 246.0 | 240.4 | 0.977 | 0.238 | 635.2 |

Average property ranges are shown below in **Table 6** (note: these now use a 10% porosity cut-off following further work). The mean values are from the two on field wells with complete penetrations (all were dry holes and 42/25-1 TD'd early within Bunter sandstone). However, due to the limited number of offset wells on the field, additional off structure offset wells were also included in to provide an appropriate property range. All wells included have good quality data and show little or no evidence of halite cementation.

Table 6 - Expected parameter ranges for P10, Mean and P90.

| Parameter | P10 | Mean | P90 |
|---------------------------------------------------------------------------------------------|--------|--------|--------|
| Net to gross | 74 % | 95 % | 97 % |
| Porosity | 16.4 % | 22.5 % | 24.1 % |
| Permeability | 100 mD | 300 mD | 500 mD |
| Note: Net reservoir is rock with $V_{cl} < 0.2$ and porosity (both density & sonic) > 0.1 | | | |

The parameter ranges in **Table 6** are predicted average reservoir properties for a penetration of the entire Bunter Sandstone Formation and are representative of what might be expected in a single new well. A campaign average (i.e. over all wells expected to be drilled) would have a much smaller range.

Outside of structure (and seismic phase reversal), wells show varying degrees of halite cementation that can be flagged from log data. The effect on porosity has been mapped out and included within in the static model.

4.0 Seal Characterisation

Containment is a fundamental component of successful long-term storage of CO₂. Endurance is a structural trap and the overburden above the reservoir has undergone rigorous analysis to ensure containment can be delivered. This has taken several forms including developing an understanding of the seals, their lateral continuity, thickness and properties, as well as interpreting and evaluating faulting present in the overburden (discussed in Geophysical Model KKD).

Above the reservoir interval at Endurance, the overburden is dominated by seal lithologies (**Figure 4**). Immediately overlying the Bunter Sandstone Formation, the lowermost seal is the Röt Clay which is ~10m of mudstone, followed by ~100m of Röt Halite. The Röt Halite package is laterally consistent and comprises 3 main units. The Röt Halite 1 (~75m thickness) which is a mainly halite with occasional, anhydrite-rich sections. Röt Halite 2 is a less halite dominated, just less than ~20m in thickness and Röt Halite 3 above returns to halite dominated with a more gradational top and base.

Above the Röt Clay and Röt Halite, which are considered to be Endurance's primary seal, lies shales of the Triassic Dowsing, Dudgeon and Triton Formations, with the evaporites of the Muschelkalk Halite and the Keuper Anhydrite intercalated between. Above the Haisborough Group, the shales of the Winterton Formation occasionally contain a thin <5m coarser clastic interval, the Rheatic Sandstone Member. However, this appears to be laterally inconsistent in the area, shaling out in some wells. Above this lies the Jurassic age Lias clay/silt mudstones which extend up to seabed over the central area of the structure (**Figure 4**).

Depositional understanding of the sealing lithologies above the Bunter Sandstone reservoir support their lateral continuity in the Endurance area. Sedimentological and petrographic work undertaken by Blackburn & Robertson (2014) on the core data from well 42/25d-3 determined that the Röt Clay and the succeeding Röt Halite have been deposited in a playa lake environment. Geluk et al. (2018) states that in Late Olenekian–Early Anisian times, the Southern Permian Basin area was episodically inundated by marine water that entered the basin from the Tethys via the Silesian gate in SE Poland (Bachmann et al. 2010). Under dry climatic conditions, the evaporites of the Röt Formation were deposited in partially restricted basins (as shown in image b of **Figure 11**).

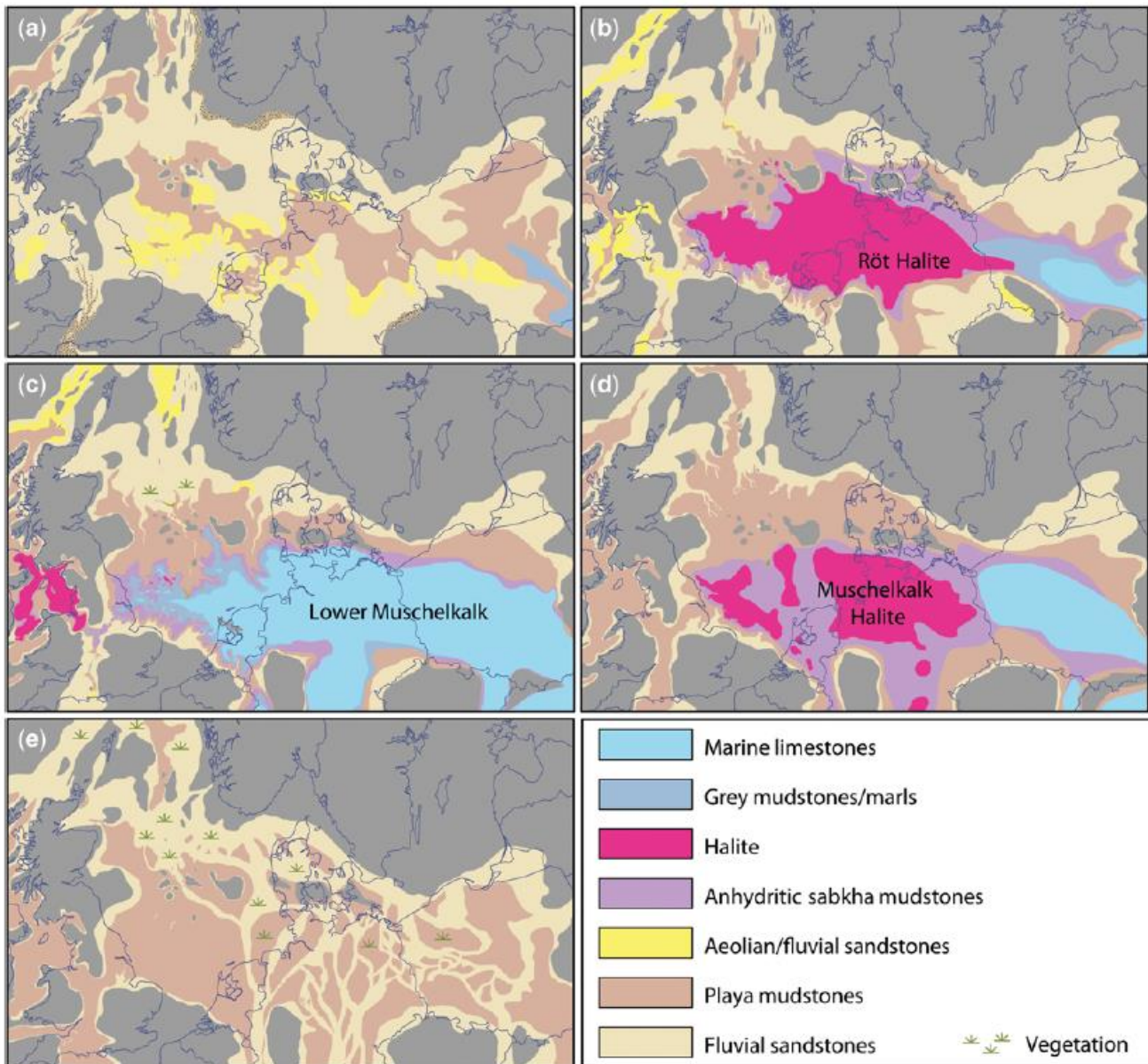
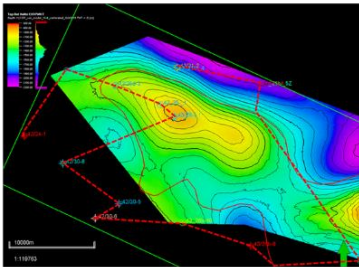
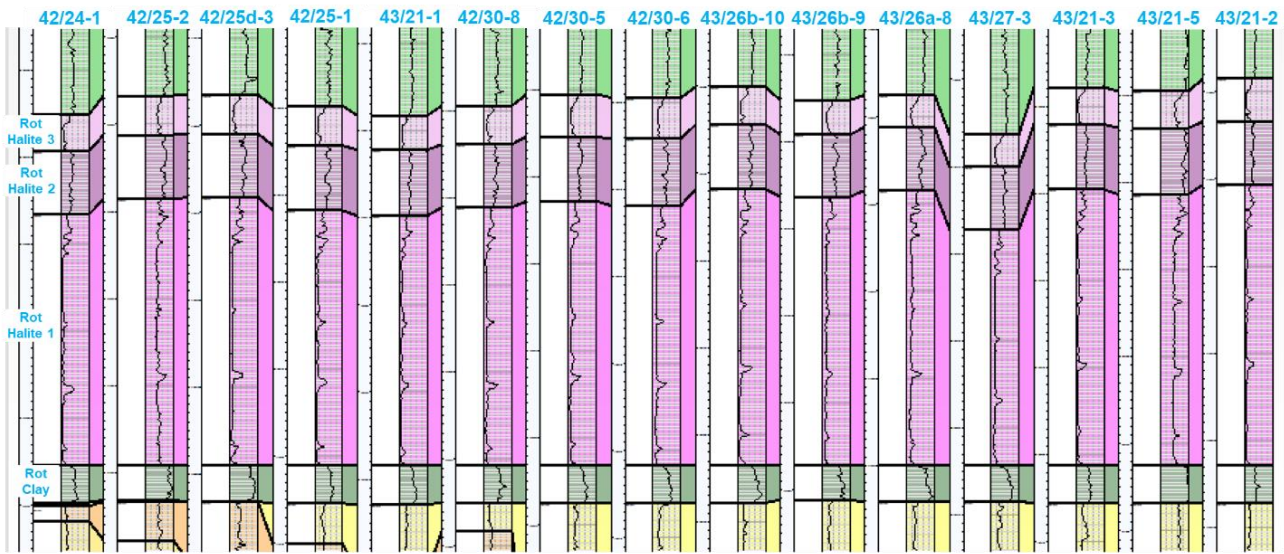


Figure 11 - Illustrative Triassic palaeogeographical reconstructions (after McKie 2017): (a) Main Buntsandstein (Olenekian) fluvial–aeolian deposition within continental basins; (b) Röt (Lower Anisian) restricted marine connection and evaporites; (c) Lower Muschelkalk marine flooding (Anisian); (d) Middle Muschelkalk basin restriction and evaporate precipitation; and (e) Schilfsandstein (Middle Carnian) expansion of Fennoscandian drainage in response to regional climate wettening. (from Geluk et al., 2018)

A review of the well log data also supports lateral continuity of the Röt Clay and Halite seals. The well correlation indicates relative homogeneity between the wells on structure and those encircling it (**Figure 12**).

GR (0-150 gAPI)



Rot Clay & Rot Halite well correlation both on and encircling the structure (red dashed line on map below) Depth MD (m). Flattened on Top Rot Clay.

Top Rot Halite Structure Map with well correlation both on and encircling the structure (red dashed line)

Figure 12 - Röt Clay and Röt Halite well correlation.

An Elemental Capture Spectroscopy (ECS) log covers the Röt Clay section and there are some points within the Röt Clay and Röt Halite core from well 42/25d-3 that were analysed petrographically, with scanning electron microscopy (SEM) and bulk x-ray diffraction (XRD). Compositionally, the ECS log identifies three key components in the Röt Clay: clay, quartz and feldspar, and carbonate. The XRD analysis points are shown in **Figure 13** below, which identified illite as the dominant clay mineral and a significant carbonate component (up to 27%).

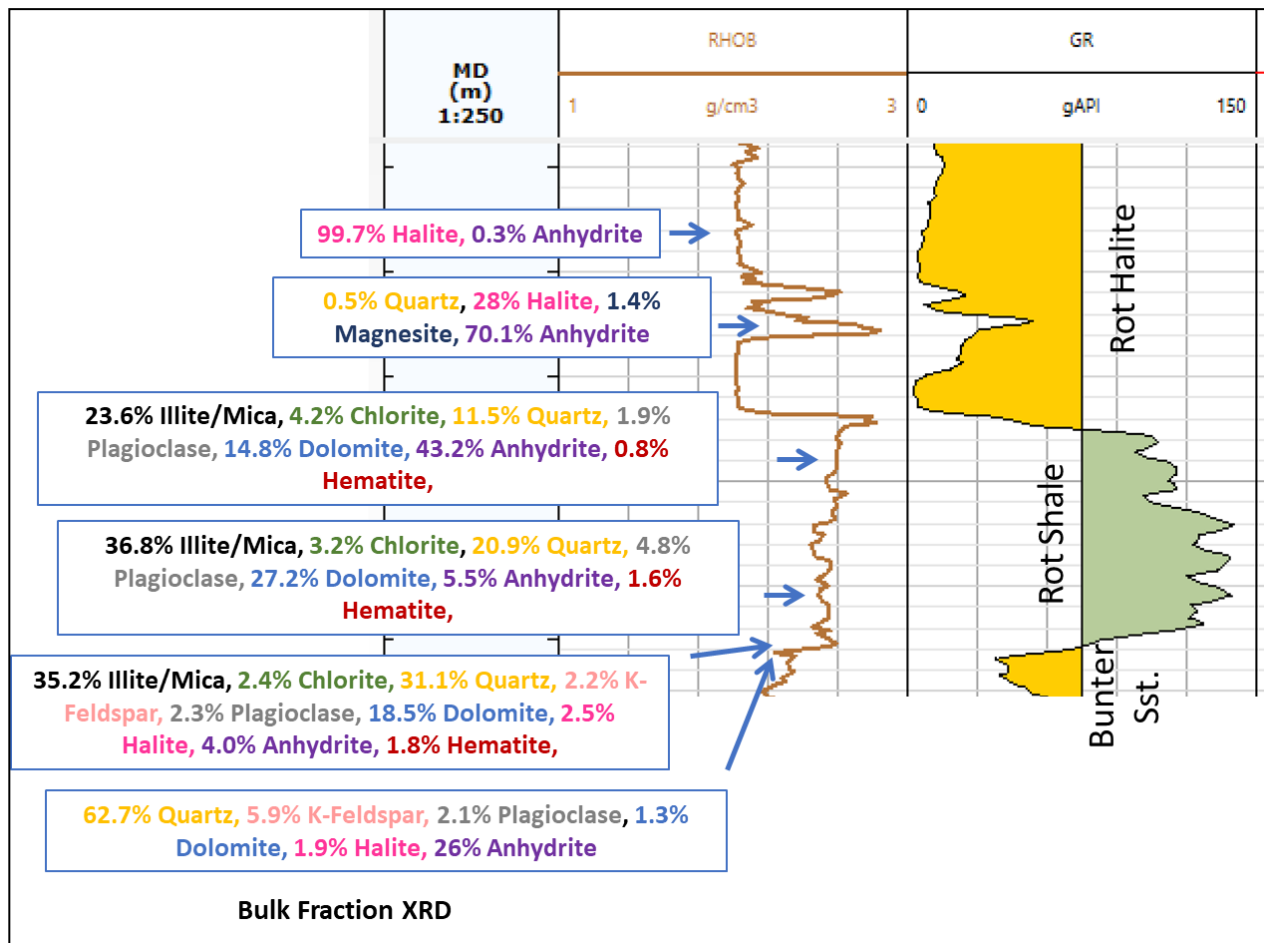


Figure 13 - 42/25d-3 Density and GR logs highlighting Röt Clay/Shale and Röt Halite sections with corresponding XRD measurements from core.

Physical properties were also measured/calculated within the Röt Clay using core from well 42/25d-3. Plug measurements from the core were taken in this interval, although there is some uncertainty on data quality due to issues with plug cleaning. The mean core porosity is 14.8% (Range: 11 – 20%).

Nuclear magnetic resonance (NMR) porosity and permeability logs were also acquired. The NMR porosity (Figure 7) does not require core calibration and has smaller vertical resolution than core and density, although it may not resolve the very smallest of pores in a clay. Porosity from density was also calculated and there is relatively close agreement from the three porosity methods.

Core measurements (with the cleaning issues noted above) and NMR permeability acquired over the Röt Clay (Figure 8) indicate a change from the relatively high porosity and permeability of the top of the Bunter Sandstone to that of the Röt Clay. The NMR log “sees” some larger pores in the clay and calculates some permeability in these areas (between 0.01 and 0.1 mD). However, the section dominantly shows sealing properties, with the upper section of the Röt Clay in 42/25d-3 being particularly tight. This section is overlain by the impermeable unit of the Röt Halite 1.

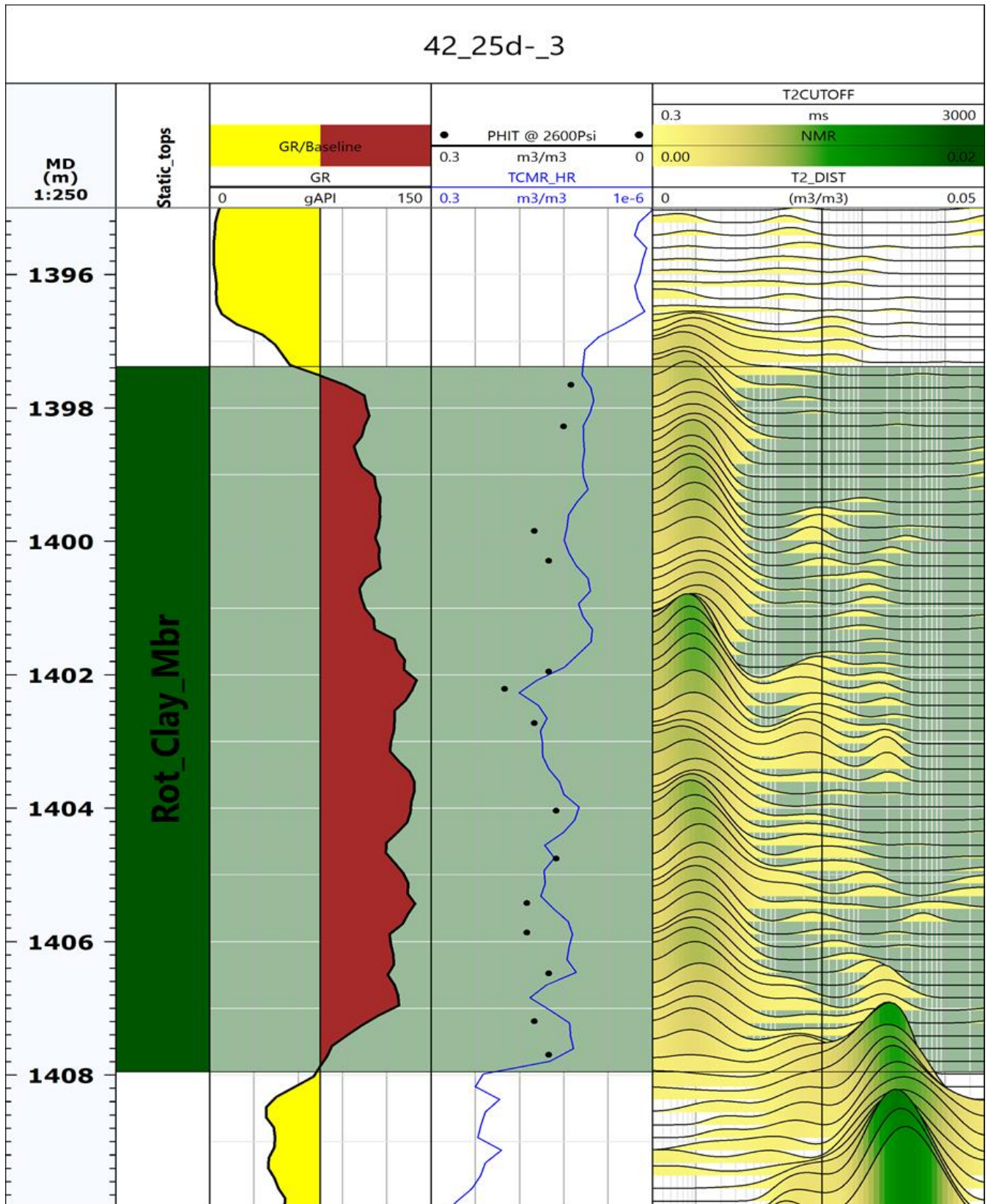


Figure 14 - Porosity measurements and T2 distributions from the NMR log over the Röt Clay clastic seal in 42/25d-3.

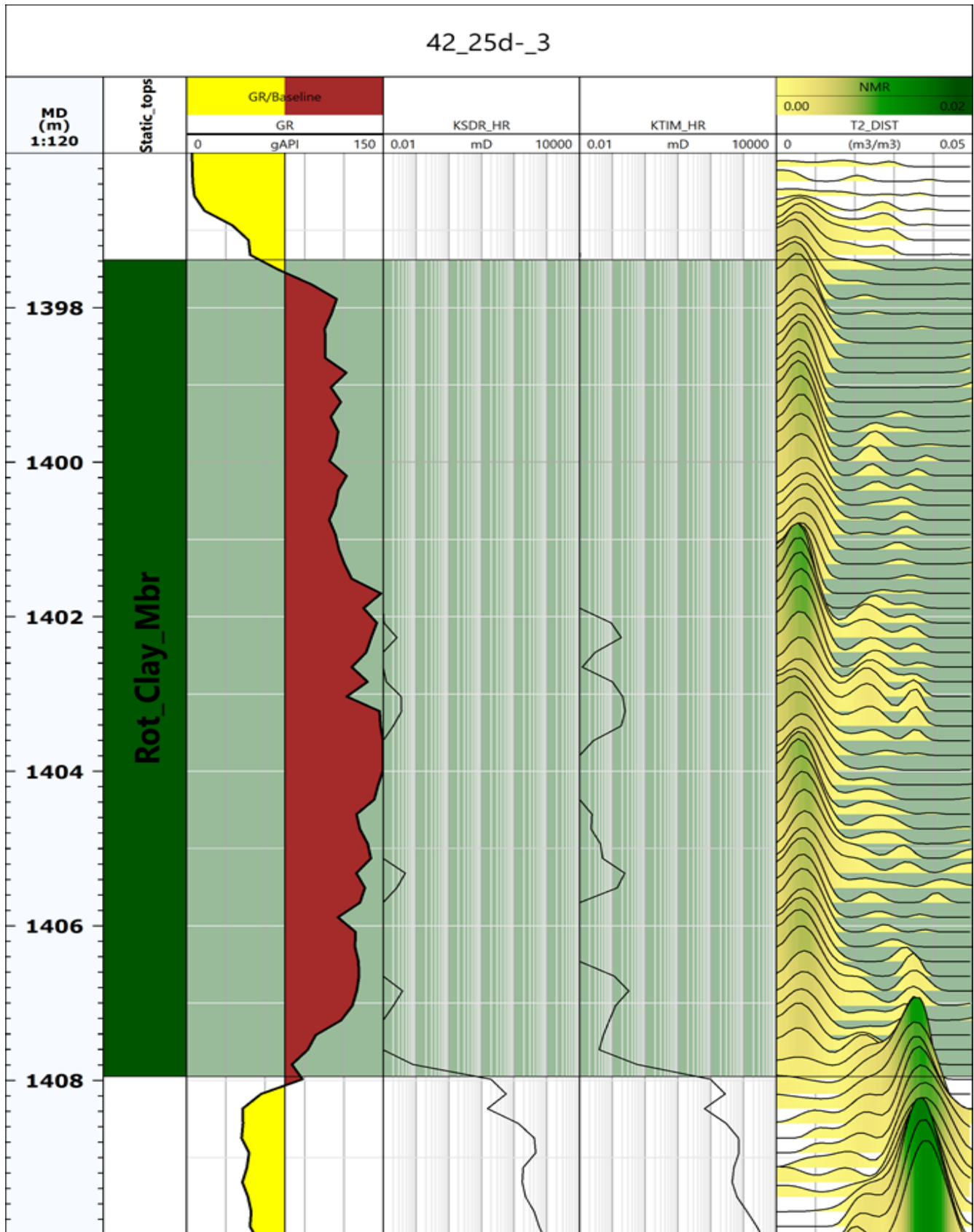


Figure 15 - Permeability measurements and T2 distributions from the NMR log over the Röt Clay clastic seal in 42/25d-3.

5.0 Static Modelling

The geological studies described above provide the stratigraphic and depositional framework, which in combination with the petrophysical rock properties and the structural framework provided via the geophysical interpretation (see Geophysical Model KKD), enable the construction of a 3D geocellular static model. The aim of the static modelling is to build geologically realistic models that capture subsurface uncertainty and quantify its impact on CO₂ injection and brine offtake scenarios.

5.1 Introduction

The static model was built in Schlumberger's Petrel software. The model incorporated insights from the lithotype core study, reprocessed seismic data and regional analogues. The model was designed to incorporate log-scale heterogeneity to better characterise the injected CO₂ plume in reservoir simulation and optimise the development scheme (CO₂ injection and brine production) for Endurance CO₂ store. The purpose of the Endurance model is to have a tool to assess the impact of the static and dynamic reservoir uncertainties on different development options. The key static uncertainties include:

- Permeability
- Net-to-gross (NTG)
- Bulk rock volume (BRV) (structural depth and gross thickness)
- Fault, segment and lateral continuity
- Porosity
- Reservoir architecture (vertical baffle extent)
-

5.2 Area of Interest

The area of interest (AOI) of the model, shown in **Figure 16**, is 50.5km by 23.9km and was chosen to be big enough to cover the 13 surrounding wells that penetrated the Bunter Sandstone and extend to the east to include the seabed outcrop that overlies a Zechstein salt diapir, 14Km SE of the Endurance structure. The outcrop has been included to study the possibility of connate water to flow through the outcrop during CO₂ injection phases. Vertically, the model AOI includes the Röt Clay down to the base of the Bunter Sandstone. The model box coordinates are shown in **Figure 17**.

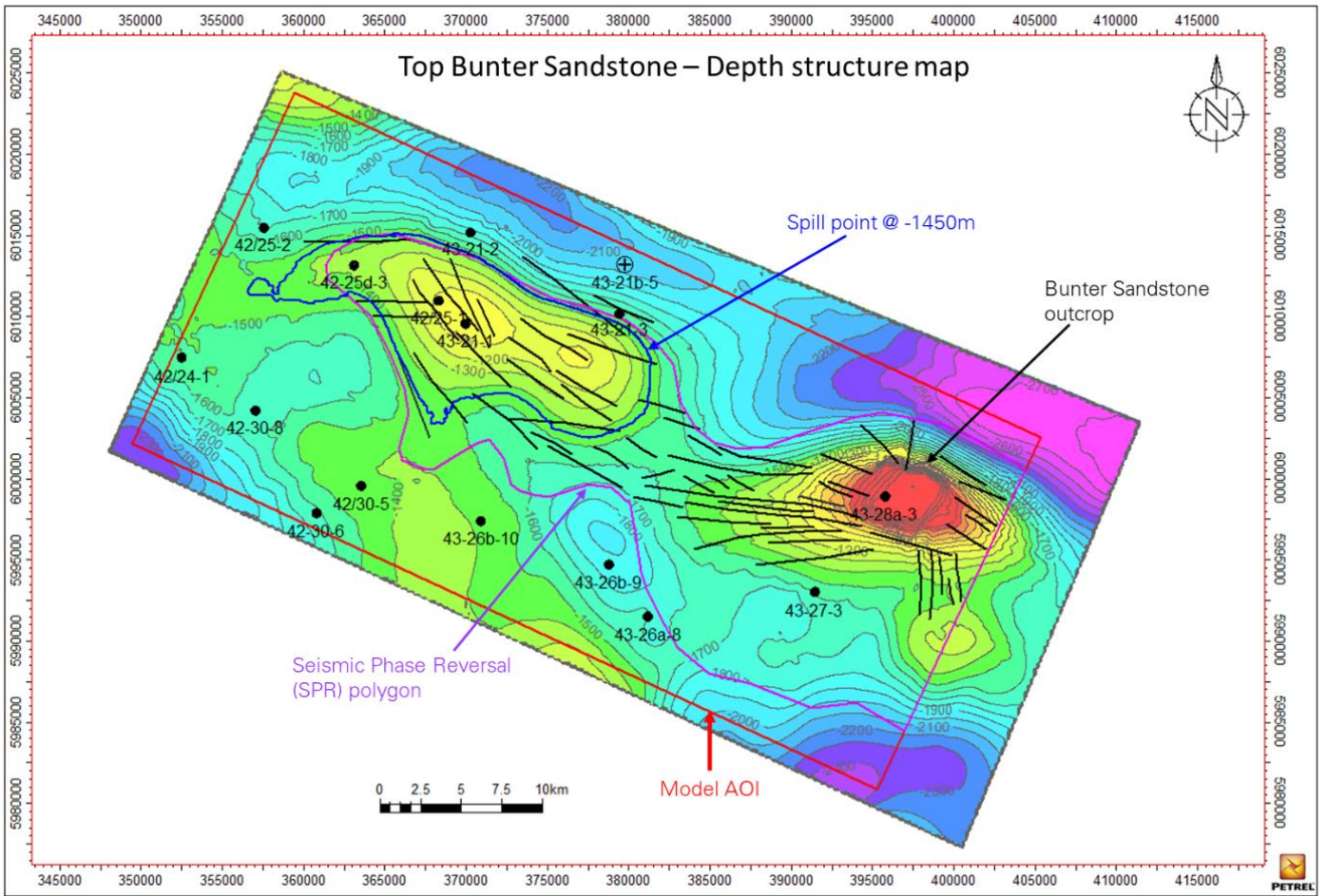


Figure 16 - Top Bunter Sandstone (top reservoir) depth structure map showing well locations and seismic phase reversal (SPR) polygon.

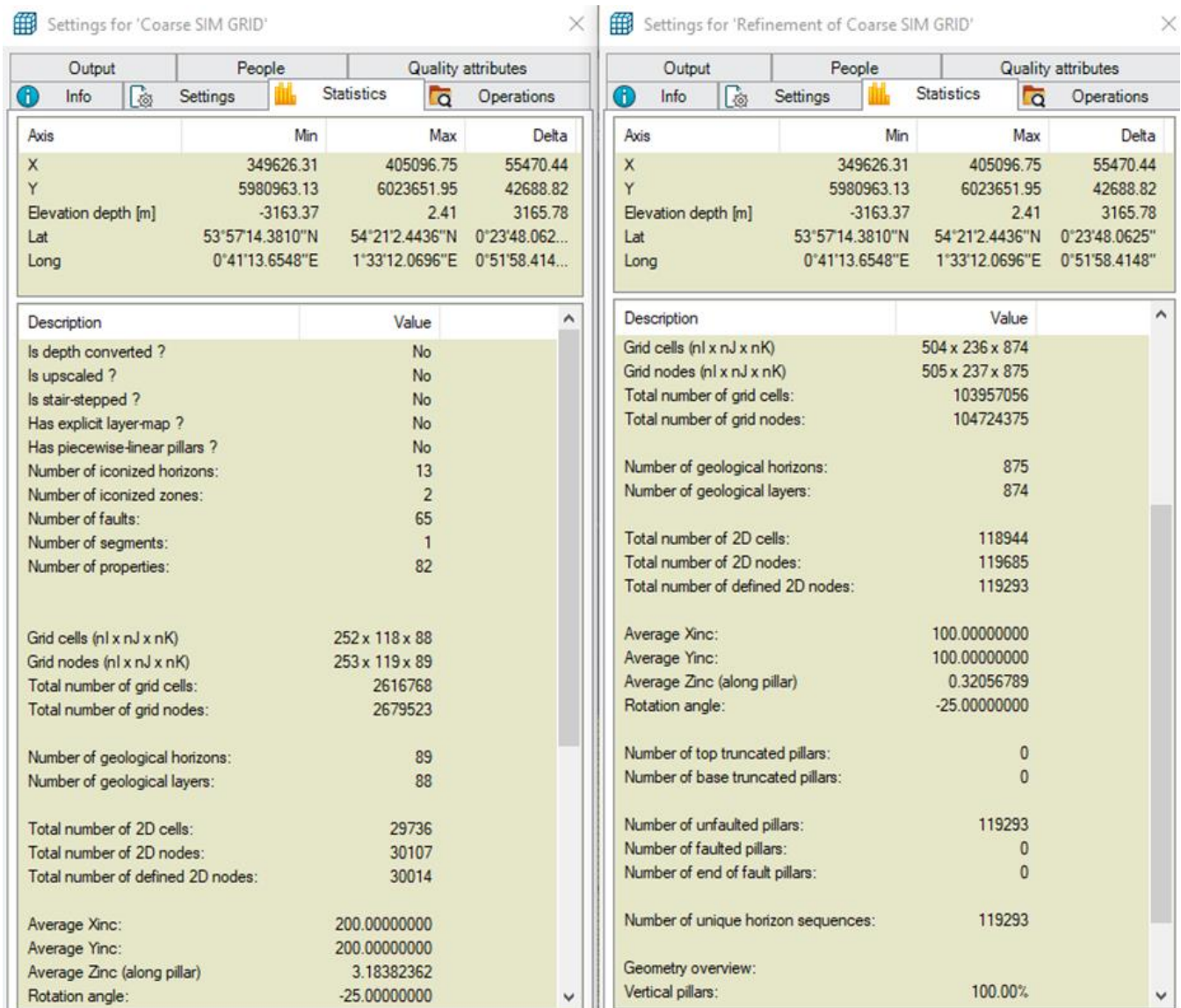


Figure 17 - Model box definition.

5.3 Structural Model

Structural modelling was performed in two steps:

Created the simulation grid using the workflow called '3D SIM GRID 200X200X3m'

Created the geological grid by refining the simulation grid.

Structural modelling is based on the input data described in previous sections and the Geophysics Model KKD. It includes seismic interpretation of surfaces (Top Bunter Sandstone and Top Bunter Shale), which were used to constrain the grid. The static model does not contain any faults, hence simple grid was implemented with the above two surfaces forming the grid envelope.

5.3.1 Fault Modelling

No faults were explicitly modelled into the grid. As discussed in the Geophysical Model KKD, most of the overburden faults appear to detach on the Röt Halite above the reservoir. The few visible faults that can be seen in the seismic on top of the Bunter Sandstone reservoir have significantly small throw and don't appear to fault the entire reservoir, hence these have not been included in the structural modelling. These faults, along with other fault lineaments mapped at the top of the Bunter Sandstone have been used as transmissibility modifiers in the simulation grid (see Dynamic Model KKD).

5.3.2 Create Simple Grid

The simple grid is based on the Top Bunter Sandstone and Top Bunter Shale surfaces to define the top and base of the grid. Both surfaces have been defined as conformable. The grid boundary is the AOI as discussed above. The grid has been given a -25° rotation to align with the structural trend, and both X and Y increments have been set to 200m.

5.3.3 Horizon Modelling/Make Horizons

As described above, only two surfaces (Top Bunter Sandstone and Top Bunter Shale) have been used to constrain the model. In make horizons process, the horizons were modelled as conformable and respective well tops used to tie the horizons.

5.3.4 Zone Modelling/Make zone

The Make zone process was used to define the geological sub-zonation (isochores) of the Bunter Sandstone reservoir (**Figure 18**). The isochores were generated based on well tops. The main purpose of the zone modelling was to capture the potentially baffling facies identified in core.

Primary Store Geological Model and Report

The screenshot shows the 'Make zones' software interface. At the top, it indicates the calculation will be performed in the selected stratigraphic interval: 'BUNTER_L3b- BUNTER_SHALE_FM'. Below this, there are tabs for 'Zones', 'Settings', 'Well adjustment', and 'Uncertainty'. The main area displays a table of zones for 'BUNTER_L3b (Reservoir_Tops_Oct 19_Plus_Bunter_cemented_intervals)'. The table has columns for Name, Color, Input type, Input, Volume correct, and Status. Below the table, there are settings for 'BUNTER_SHALE_FM (Reservoir_Tops_Oct 19_Plus_Bunter_cemented_intervals)' including 'Build from', 'Volume correction', and 'Build along' options.

| Name | Color | Input type | Input | Volume correct | Status |
|--------------------------|-------|-------------|--------------------------------------------------------------------------------|----------------|--------|
| Bunter_Z6 | | Isochore | Bunter_Z6 | Yes | Done |
| P_C_Cem_1_Top | | | P_C_Cem_1_Top (Reservoir_Tops_Oct 19_Plus_Bunter_cemented_intervals) | | Done |
| Bunter_Carb_Cemented_2 | | Isochore | Bunter_Carb_Cemented_2 | Yes | Done |
| P_C_Cem_1_Base | | | P_C_Cem_1_Base (Reservoir_Tops_Oct 19_Plus_Bunter_cemented_intervals) | | Done |
| Bunter_Z5 | | Conformable | | Yes | Done |
| P_C_Cem_2_Top | | | P_C_Cem_2_Top (Reservoir_Tops_Oct 19_Plus_Bunter_cemented_intervals) | | Done |
| Bunter_Carb_Cemented_1 | | Isochore | Bunter_Carb_Cemented_1 | Yes | Done |
| P_C_Cem_2_Base | | | P_C_Cem_2_Base (Reservoir_Tops_Oct 19_Plus_Bunter_cemented_intervals) | | Done |
| Bunter_Z4 | | Conformable | | Yes | Done |
| Het_Silt_P_C_Cem_1_Top | | | Het_Silt_P_C_Cem_1_Top (Reservoir_Tops_Oct 19_Plus_Bunter_cemented_intervals) | | Done |
| Heterolithics_Cemented | | Isochore | Heterolithics_Cemented | Yes | Done |
| Het_Silt_P_C_Cem_1_Base | | | Het_Silt_P_C_Cem_1_Base (Reservoir_Tops_Oct 19_Plus_Bunter_cemented_intervals) | | Done |
| Bunter_Z3 | | Conformable | | Yes | Done |
| Lower_Zone_Top | | | Lower_Zone_Top (Reservoir_Tops_Oct 19_Plus_Bunter_cemented_intervals) | | Done |
| Lower_Zone Cemented | | Isochore | Lower_Zone Cemented | Yes | Done |
| Lower_Zone_Base | | | Lower_Zone_Base (Reservoir_Tops_Oct 19_Plus_Bunter_cemented_intervals) | | Done |
| Bunter_Z2 | | Conformable | | Yes | Done |
| Lower_Fine_Top | | | Lower_Fine_Top (Reservoir_Tops_Oct 19_Plus_Bunter_cemented_intervals) | | Done |
| Lower_Zone_Fine_Cemented | | Isochore | Lower_Zone_Fine_Cemented | Yes | Done |
| Lower_Fine_Base | | | Lower_Fine_Base (Reservoir_Tops_Oct 19_Plus_Bunter_cemented_intervals) | | Done |
| Bunter_Z1 | | Isochore | Bunter_Z1 | Yes | Done |

Build from: Top horizon
 Volume correction: Proportional correction
 Build along: Vertical thickness (TVT) Support steep slopes

Figure 18 - Zone modelling stage.

5.3.5 Layering

The layering of the zones was established based on the average thickness of the sub-zones, aiming for a thickness of 3m for vertical grid cell resolution (**Figure 19**). Cell thickness of 3m was chosen as a compromise between overall number of cells and computational time of dynamic simulation.

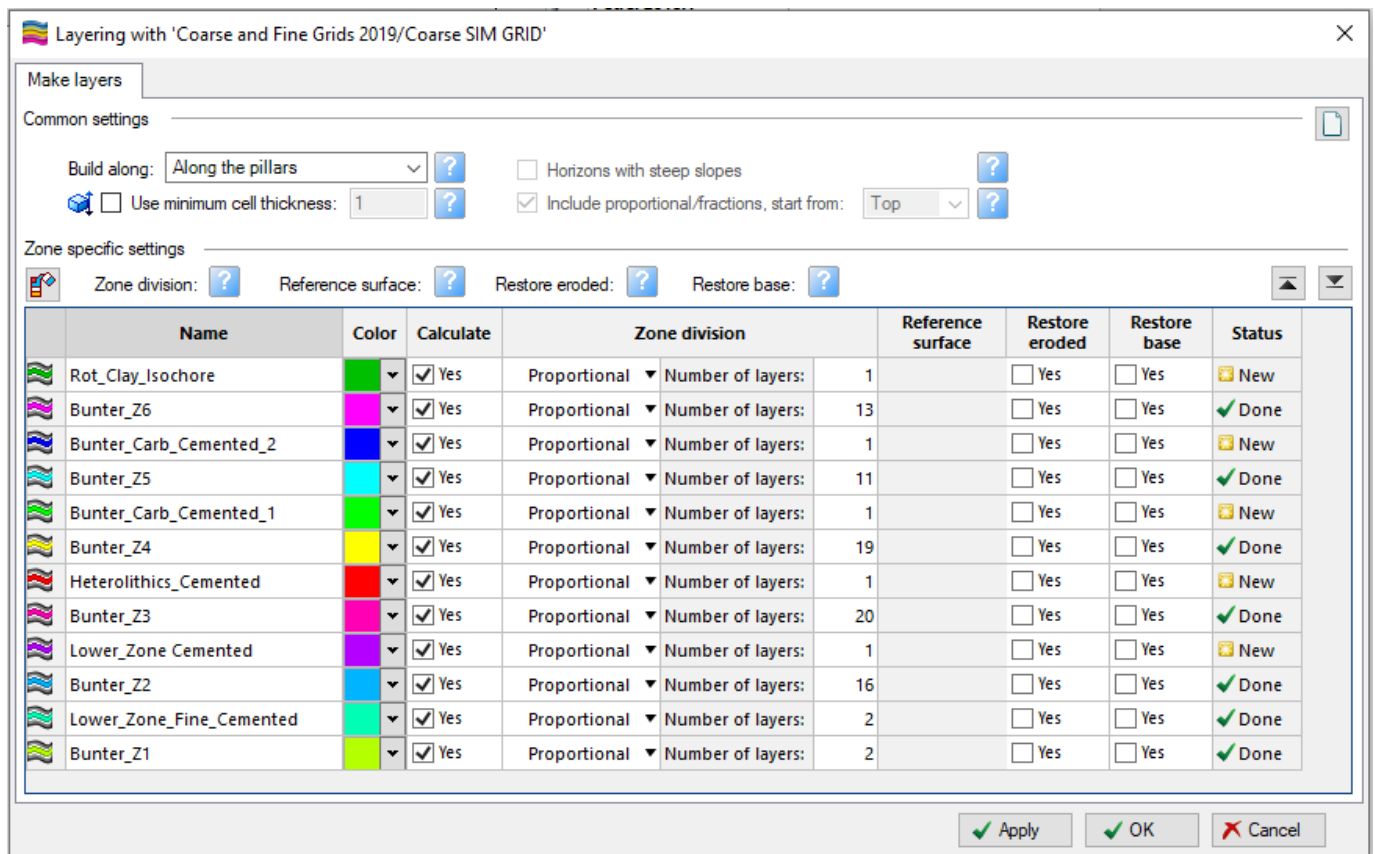


Figure 19 - Grid layering.

5.4 Grid

Two Grids are created SIM Grid (Coarse SIM Grid) and GEO Grid (refinement of Coarse SIM Grid). In this modelling project petrophysical modelling is carried out in the refined grid and upscaled into the simulation grid (Coarse SIM Grid).

5.4.1 Well Log Upscaling

The following well logs area upscaled: Petrofacies (Petrofacies_v3), net porosity (PHIT_ALL_NET) and net reservoir (RES_NET_FLAG1). When upscaling the petrofacies logs, 'Most of' was used with no bias and no weighting. Porosity and Net-to-Gross (NTG) logs were upscaled using arithmetic average, as this yielded better results compared with the other available averaging methods. No bias and no weighting were used for the upscaling of the logs.

5.5 Facies Modelling

The objective of facies modelling was to create a set of facies that relate to reservoir properties which could be used for property distribution in the static reservoir model. Four main electro facies were picked on common logs that were available in all wells: gamma-ray, sonic, resistivity and porosity (**Table 7**). The facies are interpreted to relate primarily to post depositional diagenetic processes that created varying degrees of cementation and porosity reduction.

Table 7 - Petrofacies wireline log cut-off criteria.

| Description | Facies Definition |
|-------------------------|-------------------------------------------------------------------------------------------------|
| Heterolithic | VCL>0.2 (Clay rich) |
| Good Sand | DT>80 us/ft, VCL<0.2 |
| Partially Cemented sand | V. low GR/VCL, lower DT than good sands (<80 us/ft) |
| Plugged & Cemented | V. low DT (<60 us/ft), very low porosity (<0.05), v. high resistivity values (highest readings) |

Good sands facies and heterolithics facies which comprise fine sands, silts and shales are interpreted to be un-cemented. Good sands have the best porosity and heterolithics variable porosity. Partially cemented sands have poorer porosity, and plugged and cemented sands have the lowest porosity.

Since not all facies occur everywhere in the reservoir (e.g. the plugged and cemented facies only occur outside of the seismic phase reversal (SPR) area), each of the individual reservoir sub-zones was modelled in two steps using the SPR parameter, which splits the reservoir model into cemented and uncemented areas as facies within the model.

1. Select the zone for modelling, and in the SPR select the facies to be uncemented, select all petrofacies that occur within the zone; use the variogram settings for anisotropy defined by the lithotype sedimentology study based on likely lateral extent of the facies. The vertical variogram is computed from experimental variograms.
2. Same as above but change the SPR region to cemented and select only the petrofacies that occur within the cemented region.

An example of the modelled facies is shown in **Figure 20**.

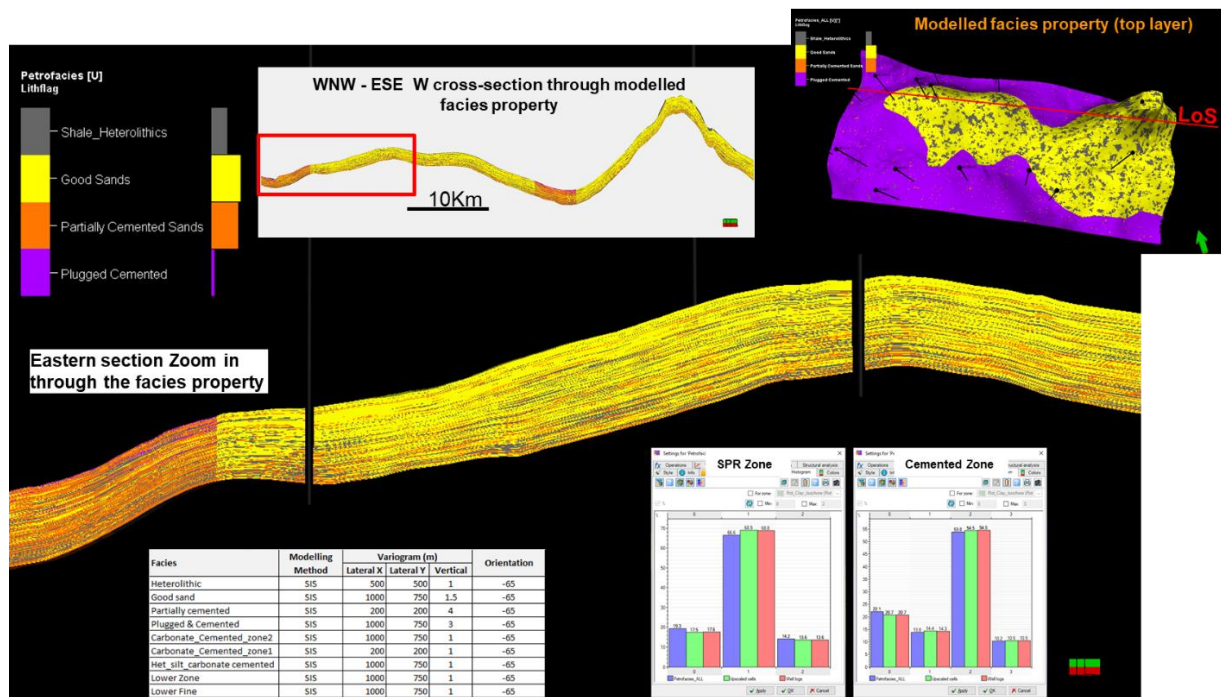


Figure 20 - Modelled facies property. Top layer of grid with line of section (inset top right), WNW – ESE cross-section through modelled facies property (top centre), Zoom through western section (centre), Proportions QC panels for cemented and uncemented regions (inset bottom right), Table with variograms used for the different petrofacies.

5.5.1 Variograms Derived from Lithotype Core Study

The cemented/potentially cemented, silt, mud and heterolithic lithotype sections were grouped to create a set of high-resolution potential baffles at 42/25d-3. As detailed previously, the lateral continuity of any of these features is doubtful on a full field scale, however, an attempt was made to examine how far potential baffled sections could extend away from the cored well (42/25d-3).

Some picks were made across the wells with a moderate level of confidence, such as Carbonate Cemented Horizon 1 (Zone 5 Top). Others such as Carbonate Cemented Horizon 2 (Zone 4 Top) were relatively low confidence picks. The uncertainty in this interpretation was addressed in the static model by allocating both potential baffles and facies using variograms.

Multiple variograms were tested and optimization carried out by iterating through to dynamic simulation tests (for example, field wide and 1km + variograms for heterolithic facies). Some results when taken forward into dynamic simulation were not immediately intuitive. An example of this was when using significantly longer variograms for the heterolithic facies resulted in greater ordering not just of potential baffles, but also of good sand and therefore greater vertical connectivity. Alternative scenarios to overcome this could potentially bring in an object-based approach.

The variogram parameters defined for populating facies in the static model are shown in **Table 8** to **Table 10** (for base case, upside and downside scenarios).

Table 8 - Variogram parameters for both potential laterally continuous baffles/nominal zone tops and also facies for base-case static model

| | Items | | Variogram (m) | | |
|-----------|--------------------|----------------------------------------------------------------------|---------------|-----------|----------|
| | | | Lateral X | Lateral Y | Vertical |
| Base Case | Potential Baffles | Carbonate Cemented Horizon 1 (Zone 5 Top) | 1000 | 750 | 1 |
| | | Carbonate Cemented Horizon 2 (Zone 4 Top) | 200 | 200 | 1 |
| | | Heterolithic/Silt/Carbonate Cemented Horizon 1 (Zone 3 Top) | 1000 | 750 | 1 |
| | | Lower Zone (Zone 2 Top) | 1000 | 750 | 1 |
| | | Lower Fine Zone (Zone 1 Top) | 1000 | 750 | 1 |
| | | | | | |
| | Facies | Heterolithic | 500 | 500 | 1 |
| | | Heterolithics included as partial net (20% mean and 0-40% range NTG) | | | |
| | | Good Sand | 1000 | 750 | 1.5 |
| | | Partially Cemented | 200 | 200 | 4 |
| | Plugged & cemented | 1000 | 750 | 3 | |

Table 9 - Variogram parameters for both potential laterally continuous baffles/nominal zone tops and also facies for upside static model.

| | Items | | Variogram (m) | | | |
|--------------------|-------------------|----------------------------------------------------------------------|---------------|-----------|----------|-----|
| | | | Lateral X | Lateral Y | Vertical | |
| Upside | Potential Baffles | Carbonate Cemented Horizon 1 (Zone 5 Top) | 1000 | 750 | 1 | |
| | | Carbonate Cemented Horizon 2 (Zone 4 Top) | 100 | 100 | 1 | |
| | | Heterolithic/Silt/Carbonate Cemented Horizon 1 (Zone 3 Top) | 100 | 100 | 1 | |
| | | Lower Zone (Zone 2 Top) | 1000 | 750 | 1 | |
| | | Lower Fine Zone (Zone 1 Top) | 1000 | 750 | 1 | |
| | | | | | | |
| | Facies | Heterolithic | | 200 | 200 | 1 |
| | | Heterolithics included as partial net (20% mean and 0-40% range NTG) | | | | |
| | | Good Sand | | 1000 | 750 | 1.5 |
| | | Partially Cemented | | 100 | 100 | 4 |
| Plugged & cemented | | 1000 | 750 | 3 | | |

Table 10 - Variogram parameters for both potential laterally continuous baffles/nominal zone tops and also facies for downside static model.

| | Items | | Variogram (m) | | |
|--------------------|-------------------|-------------------------------------------------------------|---------------|-----------|----------|
| | | | Lateral X | Lateral Y | Vertical |
| Downside | Potential Baffles | Carbonate Cemented Horizon 1 (Zone 5 Top) | 1000 | 750 | 1 |
| | | Carbonate Cemented Horizon 2 (Zone 4 Top) | 200 | 200 | 1 |
| | | Heterolithic/Silt/Carbonate Cemented Horizon 1 (Zone 3 Top) | 1000 | 750 | 1 |
| | | Lower Zone (Zone 2 Top) | 1000 | 750 | 1 |
| | | Lower Fine Zone (Zone 1 Top) | 1000 | 750 | 1 |
| | | | | | |
| | Facies | Heterolithic | 500 | 500 | 1 |
| | | Heterolithics included as non-net | | | |
| | | Good Sand | 1000 | 750 | 1.5 |
| | | Partially Cemented | 200 | 200 | 4 |
| Plugged & cemented | | 1000 | 750 | 3 | |

5.6 Petrophysical Modelling

Petrophysical modelling has been carried out to distribute Net-to-gross (NTG) and Porosity. Permeability modelling was carried out by applying the Porosity to Permeability transform directly to the modelled porosity.

5.6.1 Net-to-Gross (NTG)

Net-to-gross (NTG) has been modelled per facies, and three distinct NTG models have been created:

- Model 1: Heterolithic lithofacies have been treated as non-net and NTG is set to 0. NTG is set to 1 for all other facies.
- Model 2: Heterolithics have been treated as net reservoir with mean and range from core measurements in this type of facies;
 - Range: 0 – 40%
 - Mean NTG: 20%
- Model 3: Similar to Model 2 with larger variogram for heterolithics facies.

5.6.2 Porosity

Porosity was modelled per facies using Gaussian Random Function Simulation (GRFS) in the petrophysical module in Petrel. Facies were given the same lateral variogram ranges as used to model the facies with vertical ranges derived from experimental variograms. Variograms were orientated ESE - WNW (-65°).

Good sands across the whole Bunter Sandstone interval have a trend with porosity decreasing with increasing depth (**Figure 21**). Heterolithic facies have a lesser trend with slight porosity reduction with increasing depth. Therefore, porosity depth trends were applied for these facies during the simulation process.

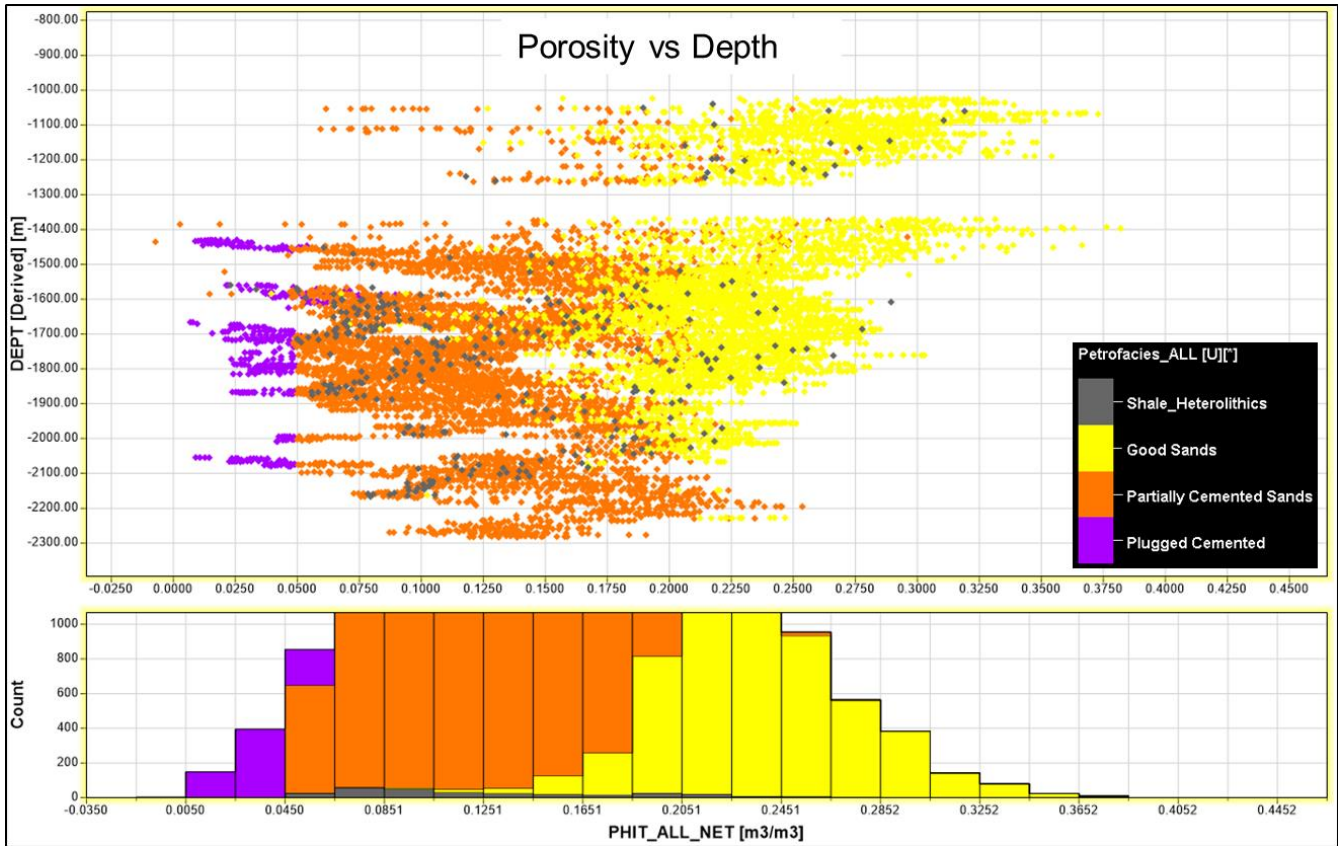


Figure 21 - Porosity versus depth graph for all four facies. The good sands (yellow) show a trend with porosity decreasing with increasing depth. Heterolithic facies (grey) have lesser trend with slight porosity reduction with increasing depth. Below is a histogram of porosity range for the four facies.

In addition to the compaction trends observed in porosity, discussed above, further analysis of the porosity distribution in the wells outside of the SPR revealed areal trends in porosity across the reservoir (**Figure 22**). It was important to incorporate these trends in the porosity model as some of areas have porosity lower than 5% across the area. Ignoring to model such changes in porosity could result in overestimating the connectivity with the regional Bunter Sandstone aquifer in some parts of the reservoir.

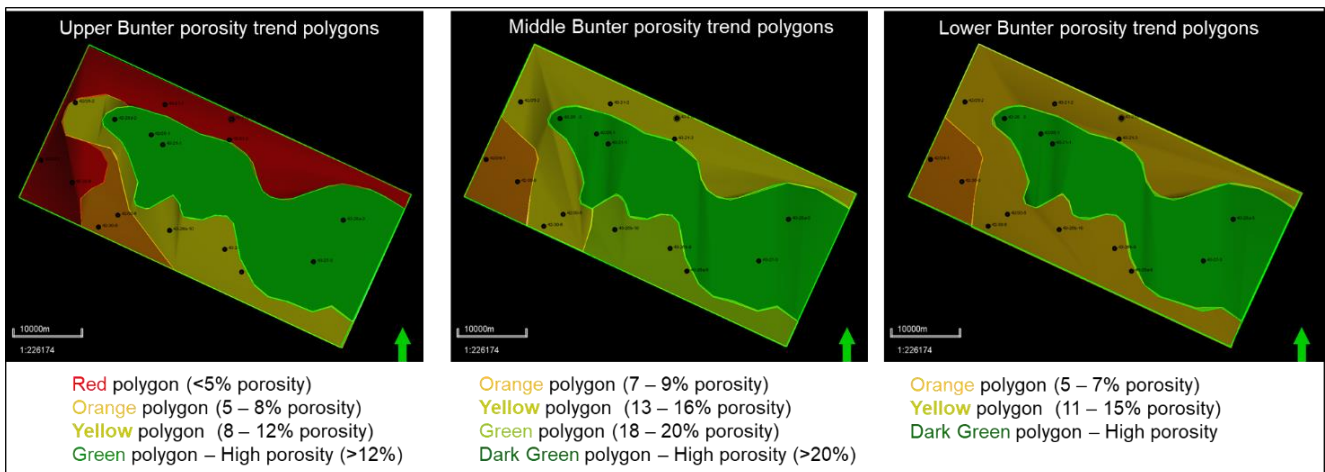


Figure 22 - Porosity trend polygons for the Upper, Middle and Lower Bunter.

Due to unavailability of density-derived porosity (PHIT_D) logs for all wells modelled (PHIT_D logs are only available in wells 42-25d-3, 42/25-1 and 43-21-1 drilled in the structure), porosity modelling used a combination of PHIT logs; PHIT_D for the three wells discussed above, and resistivity-derived porosity (PHIT_R) for wells outside of the SPR. Additionally, there is no PHIT_D available for well 43-27-3, drilled farthest east in the structure. It was therefore agreed to use sonic-derived porosity (PHIT_S) as this is the only well with porosity measurement to calibrate porosity in this part of the structure. The detailed porosity modelling workflow is described in **Figure 23**.

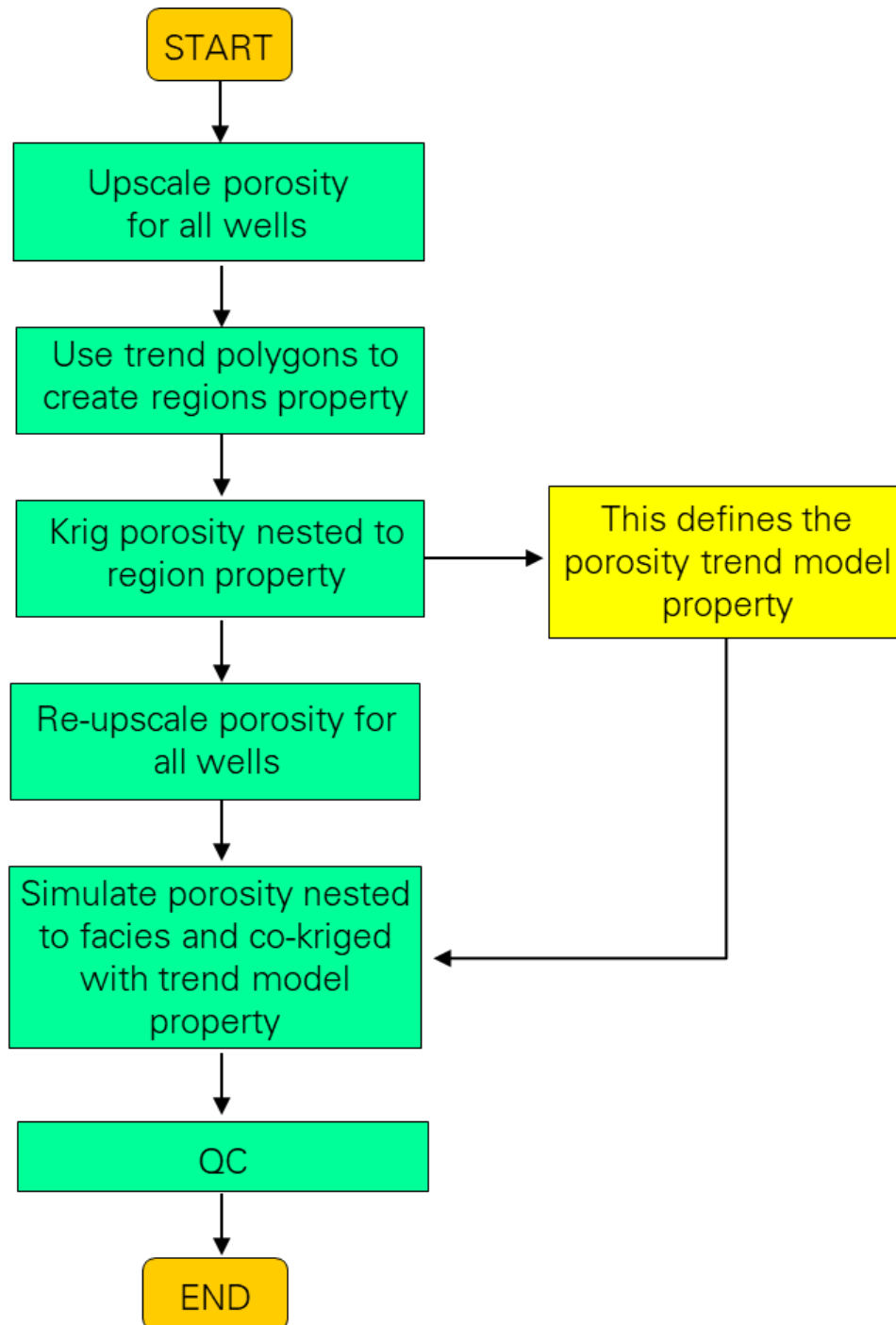


Figure 23 - Porosity modelling workflow.

5.6.3 Permeability

Permeability model has been created based on a single Porosity-Permeability transform for all facies and applied directly to the modelled porosity. The equation for this Porosity-Permeability transform is (Figure 24):

$$K = 10^{**} (4.19211 * \log_{10}(PHIT) + 5.168417)$$

The modelled permeability is shown in (Figure 25).

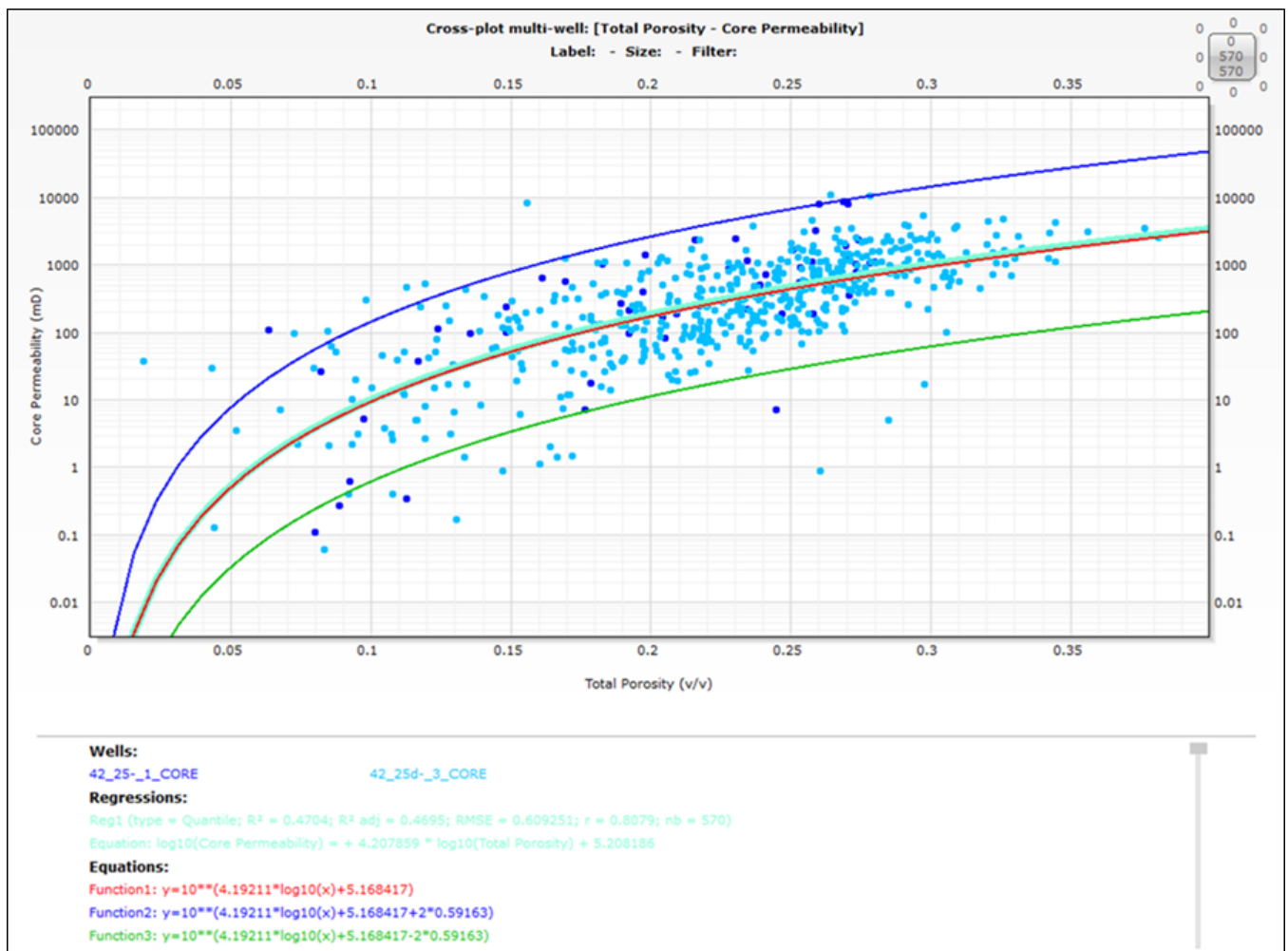


Figure 24 - Bunter Sandstone reservoir multi-well total porosity versus core permeability cross-plot.

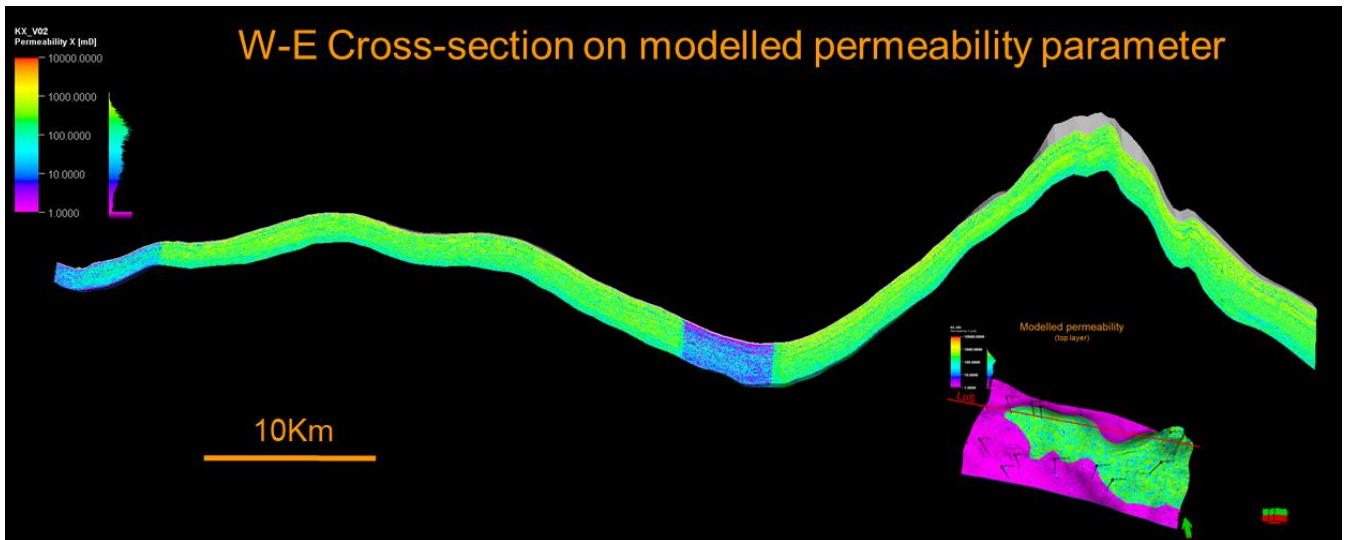
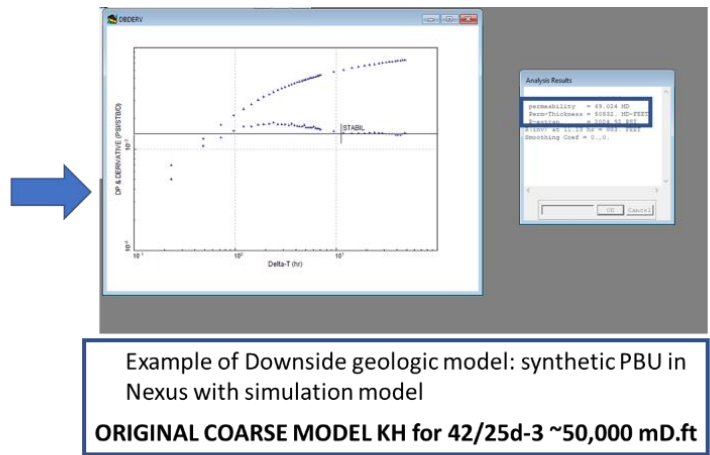
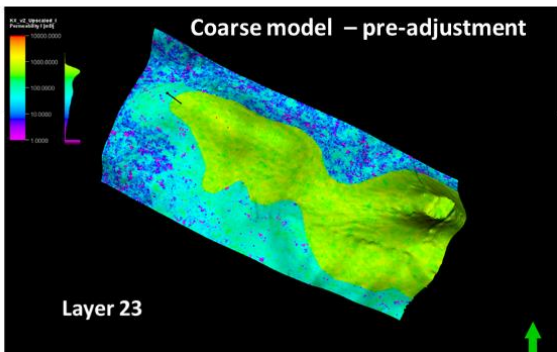
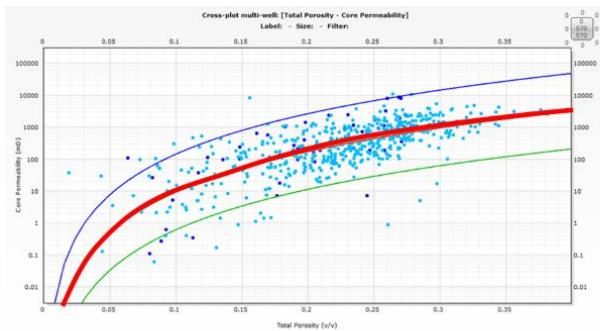


Figure 25 - Modelled permeability with top layer of grid with line of section (inset bottom right). Note low permeability area between structure and outcrop is result of position of line of section i.e. along outer edge, cutting across phase reversal. A line of section through central axis between structure and outcrop shows no significant reduction in permeability within the phase reversal.

Following the initial permeability modelling, the Porosity - Permeability transform was adjusted to better match the permeability observed in the well test on 42-25d-3 well (prior to receipt of the stressed test data) (Figure 26 and Figure 27).



Example of Downside geologic model: synthetic PBU in Nexus with simulation model
ORIGINAL COARSE MODEL KH for 42/25d-3 ~50,000 mD.ft

**Original transform $K = 10^{*(4.19211*\log_{10}(\text{poro})+5.168417)}$
 USED FOR PERMEABILITY MODELLING in FINE GRID (PRE_UPSCALING)**

Adjust poro-perm transform to match PBU K.H.

Figure 26 - Permeability modelling workflow (calibration to well test in 42/25d-3) – pre-adjustment.

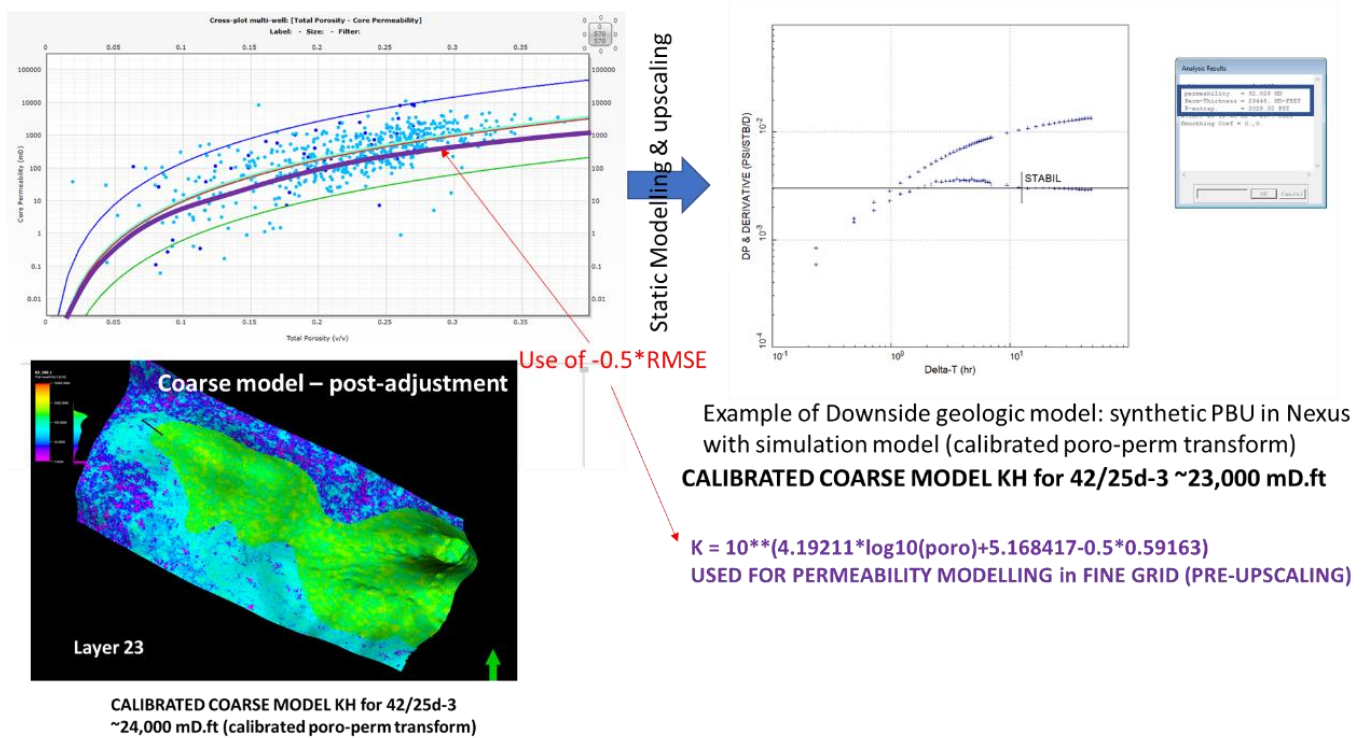


Figure 27 - Permeability modelling workflow (calibration to well test in 42/25d-3) – post-adjustment.

The adjusted transform is as follows:

$$K = 10 ** (4.19211 * \log_{10}(PHI) + 5.168417 - 0.5 * 0.59163)$$

The reason for the requirement of this adjustment was found to be in the overburden correction of the data. This is rectified in later versions of the model.

5.7 Upscaling

The modelled reservoir properties were upscaled into the SIM grid through the grid property upscaling module in Petrel. Net-to-gross (bulk volume weighted by default), was upscaled using arithmetic averaging. Porosity is volume weighted by NTG, and upscaled using arithmetic averaging. Permeability was upscaled using flow-based algorithm, finite difference, diagonal IJK tensor, with boundary condition closed to flow and extra skin of 1.

Permeability upscaling has been quality assured by carrying out single-phase tracer simulation for both fine and coarse grids (restricted to a sector of the model centred around well 42/25d-3: due to high number of active cells for the fine-scale model, Nexus simulator was not able to run) (**Figure 28**).

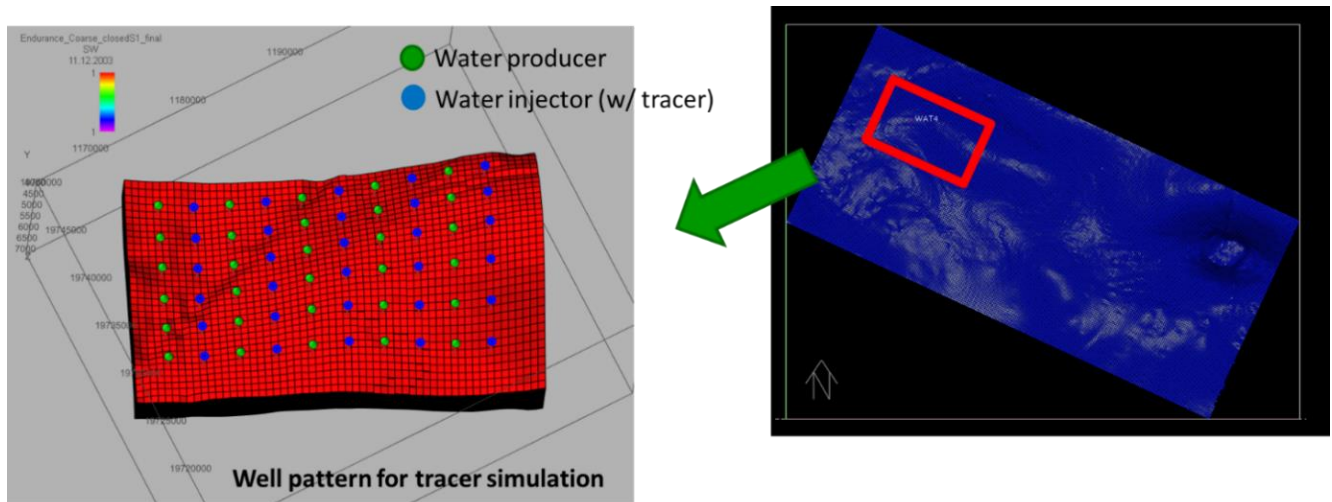


Figure 28 - Sector of the geo- and simulation grid considered for single-phase tracer modelling.

A well pattern of water producer and water injector (injected water with tracer for tracking at the producers) was created and used for simulation. Sweep patterns as well as tracer breakthrough profiles were compared to ensure that the level of heterogeneity losses was acceptable (**Figure 29** and **Figure 30**).

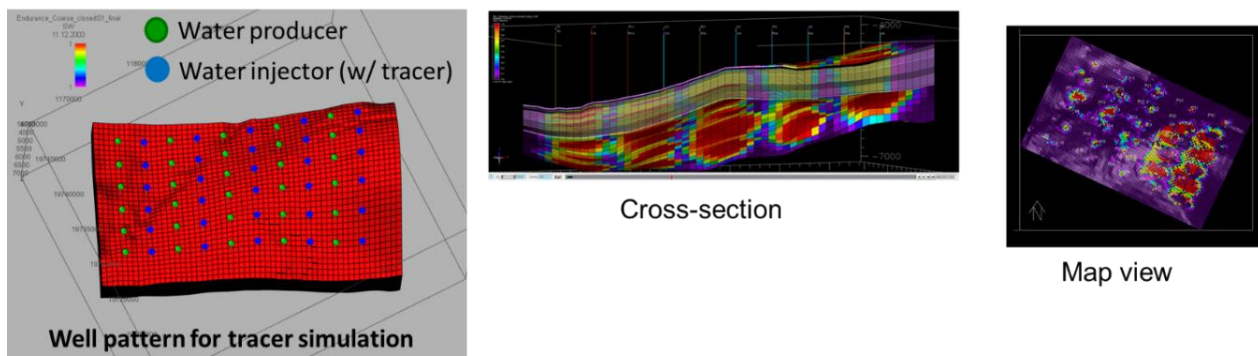


Figure 29 - Single-phase tracer modelling for Endurance (upscaling QA/Q, coarsening factor 2*2*10). Coarse scale: 200m*200m*3m NX=57*NY=35*NZ=88. Fine scale: 100m*100m*0.3m NX=114*NY=70*NZ=858

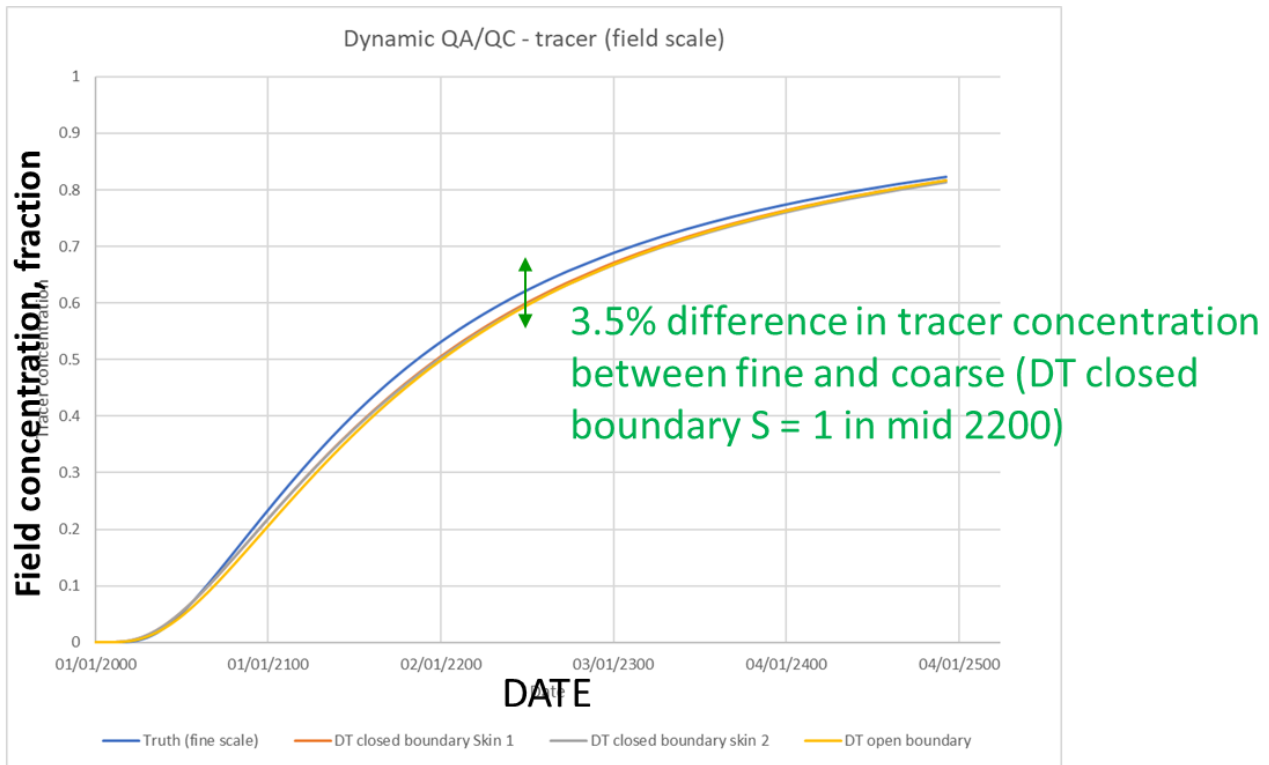


Figure 30 - Single-phase tracer modelling for Endurance (field-level tracer concentration over time for fine model and coarsened model).

5.8 Static Model QC

The static model QC was carried out at every stage of the model building process. Post petrophysical modelling and upscaling, a QC panel comparing all modelled properties versus the corresponding input data, in the fine grid and coarse grid was generated (**Figure 31** and **Figure 32**).

Primary Store Geological Model and Report

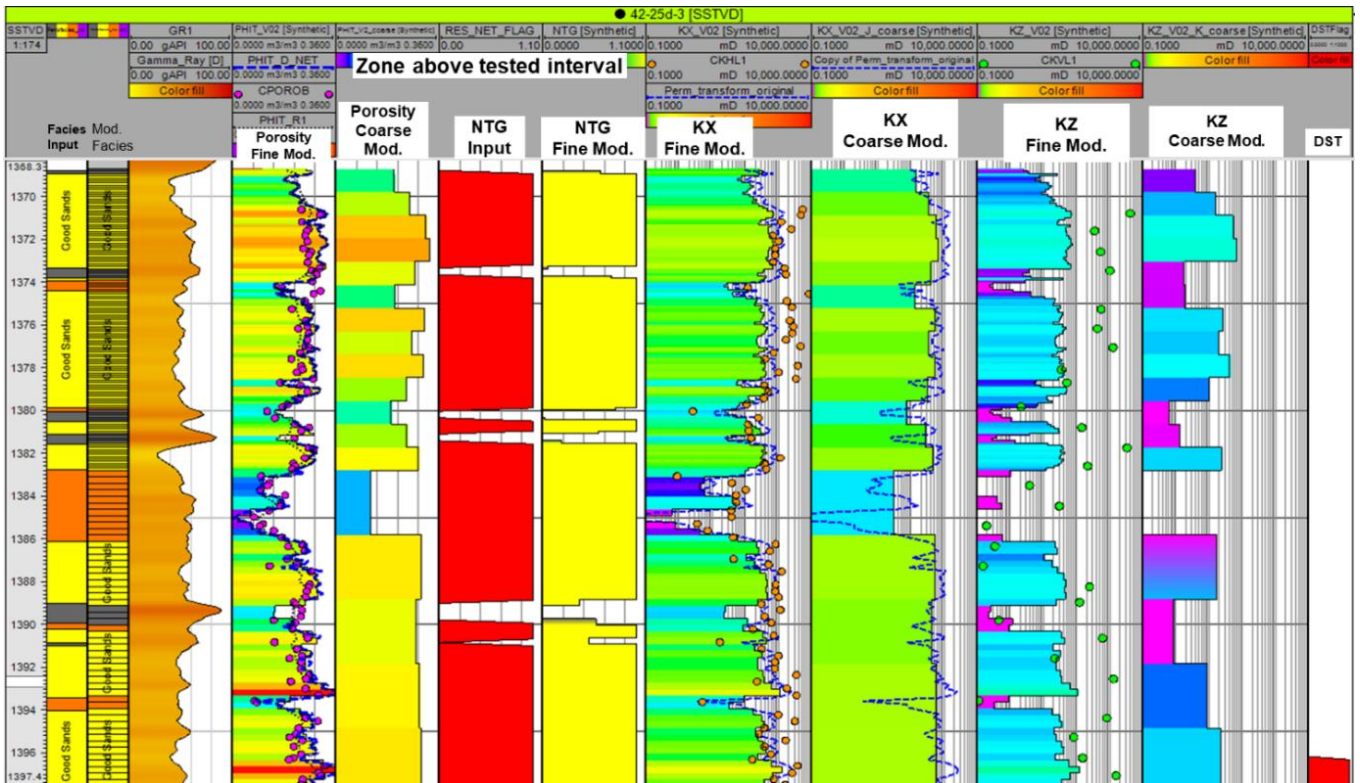


Figure 31 - QC panel over the top part of the reservoir comparing various modelled properties against input data in well 42-25d-3.

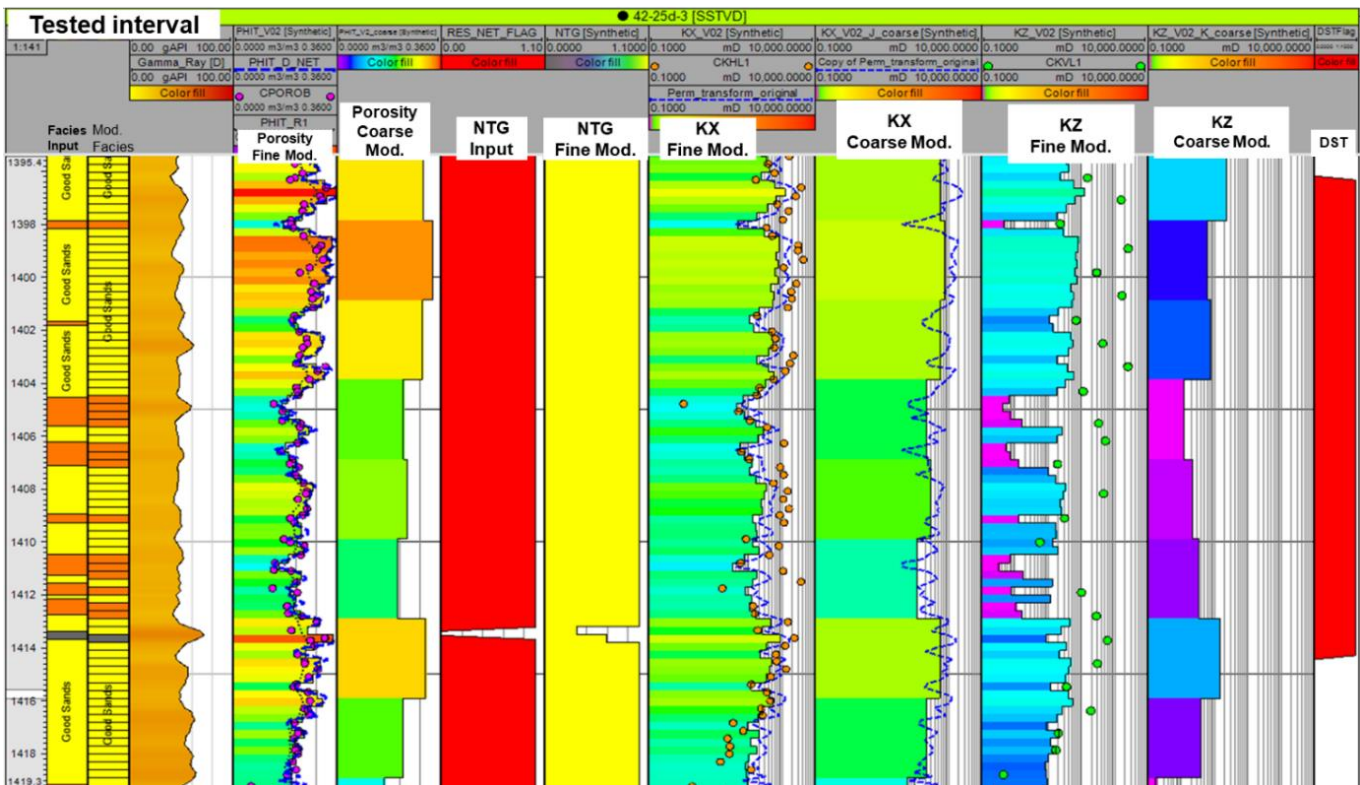


Figure 32 - QC panel over the tested interval of the reservoir comparing various modelled properties against input data in well 42-25d-3.

5.9 Fault and Segment

A set of fault lineaments were imported into the Petrel project and used to generate segments and fault transmissibility multiplier, which were used in the simulation model to test compartmentalization scenarios (see Dynamic Model KKD) (**Figure 33**).

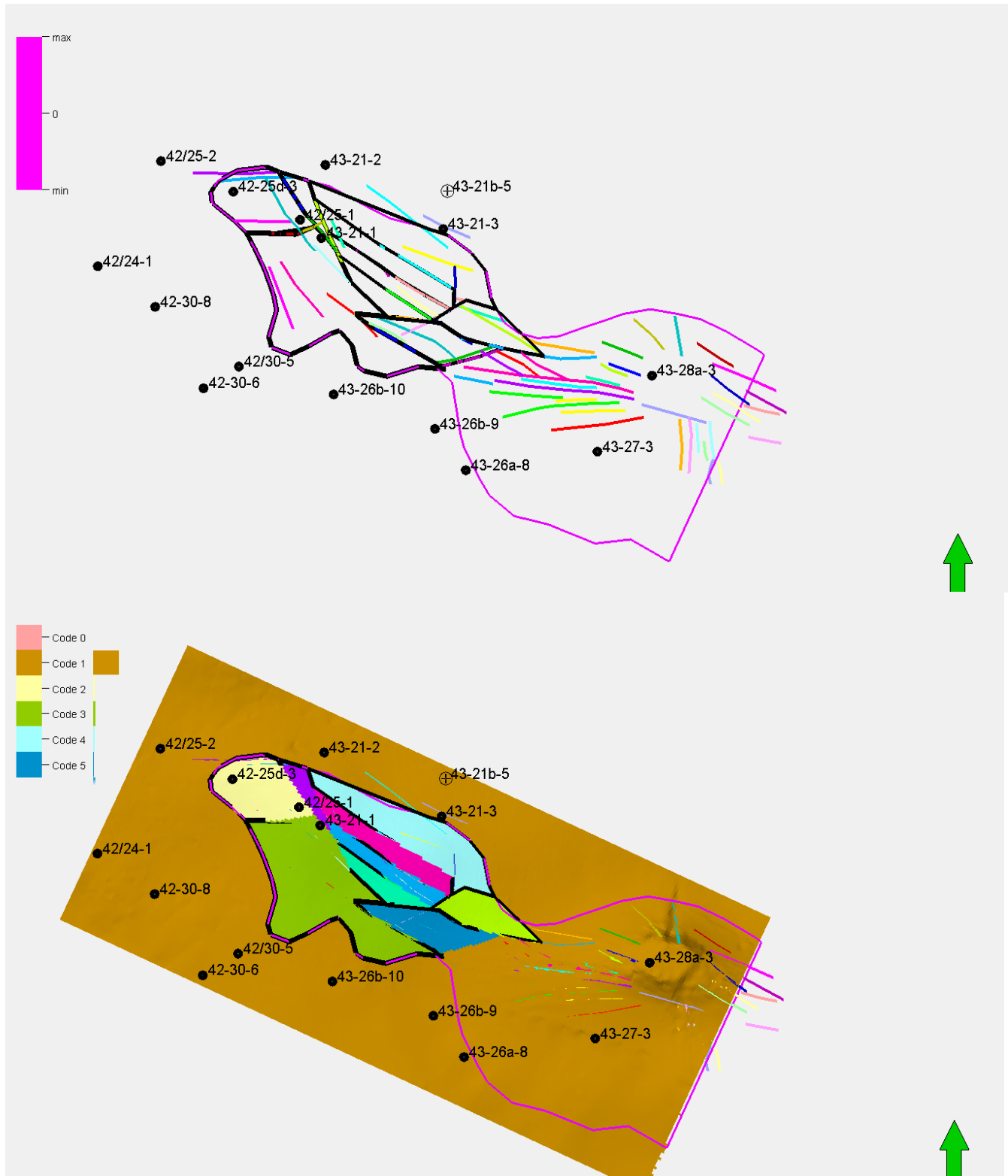


Figure 33 - Faults and conceptual segments considered for uncertainty analysis study.

5.10 Volumetrics

Volume was calculated using the grid and modelled NTG and porosity in the fine grid and compared to volumes calculated in the coarse grid, with upscaled properties. The volumes in both grids are very similar with negligible difference of 0.02% (**Table 11**).

Table 11 - Volume comparison between coarse (SIM grid) and fine grid.

| | BRV[*10 ⁶ m3] | NTG | NRV[*10 ⁶ m3] | Porosity | Net PV[*10 ⁶ rm3] | Comments |
|--------------------------|--------------------------|--------|--------------------------|----------|------------------------------|--------------------------------------------------------------------------------------------------|
| Coarse Grid Case1 | 23,448 | 0.74 | 17,383 | 0.23 | 4,083 | Heterolithic facies treated as non-net. |
| Fine Grid Case1 | 23,451 | 0.74 | 17,385 | 0.23 | 4,084 | |
| Delta (%) | 0.01 | - 0.00 | 0.01 | 0.01 | 0.02 | Difference between fine grid and upscaled properties in coarse grid is negligible. |
| | BRV[*10 ⁶ m3] | NTG | NRV[*10 ⁶ m3] | Porosity | Net PV[*10 ⁶ rm3] | Comments |
| Coarse Grid Case2 | 23,448 | 0.77 | 18,143 | 0.23 | 4,206 | Hetrolithic facies modelled as net reservoir with res. properties values from core measurements. |
| Fine Grid Case2 | 23,451 | 0.77 | 18,146 | 0.23 | 4,207 | |
| Delta (%) | 0.01 | 0.00 | 0.02 | 0.01 | 0.02 | Difference between fine grid and upscaled properties in coarse grid is negligible. |
| | BRV[*10 ⁶ m3] | NTG | NRV[*10 ⁶ m3] | Porosity | Net PV[*10 ⁶ rm3] | Comments |
| Coarse Grid Case3 | 23,448 | 0.81 | 19,011 | 0.23 | 4,372 | Hetrolithic facies modelled as net reservoir with res. properties values from core measurements. |
| Fine Grid Case3 | 23,451 | 0.81 | 19,013 | 0.23 | 4,372 | |
| Delta (%) | 0.01 | - 0.00 | 0.01 | - 0.01 | - | Difference between fine grid and upscaled properties in coarse grid is negligible. |

6.0 Conclusions

The Triassic Bunter Sandstone is the reservoir interval at the Endurance CO₂ store. It is interpreted as being deposited in a semi-arid, landlocked, gradually subsiding basin with fluvial systems terminating in playa lake, playa margin, aeolian dune and sabkha settings. Sedimentation rates were low (100m/3Ma) with considerable reworking and recycling via fluvial and aeolian processes.

A detailed lithotyping study conducted for this project, focussed on attempting to identify potential baffle/barrier lithotypes and understand their deposition to underpin their distribution within the static model. Cores 2, 3 and 4 from well 42/25d-3 were interpreted to reflect an overall fluvial-aeolian setting, with highly reworked depositional elements. While many setting-diagnostic sedimentary structures occur (climbing ripples and trough cross-bedding for fluvial, steepening upward cross-sets and adhesion ripples for aeolian), there are few to no clearly observable depositional elements. Rather, the overall effect is of an amalgam of remnant dunes, small-scale stream channels, splays and rare interfluves in a highly reworked, low accommodation space setting. There was no organic matter seen anywhere in the cores, and very rare bioturbation (insect burrows) indicating the environment was barren and hostile to life.

It is unlikely that any one depositional element is completely preserved, and therefore dimensional width/thickness relationships are unlikely to apply. However, it is clear from the decimetre-scale bed boundaries common throughout the section that any individual bedset is unlikely to extend far laterally. Potential baffles/barriers identified from lithotypes for inclusion in static modelling are cemented intervals/surfaces and heterolithic sections.

The baffles in the core that are likely to have lateral extent are cm to ~10 cm silty layers that often form half-m scale heterolithic units. These silty layers include rare bioturbation (likely insect traces), common sand filled mud cracks and are associated with small-scale rippled sands. They also occur with massive sands with flat-lying platy mudclasts, which can be assumed to be slightly remobilised thin silt layers, very locally reworked by a subsequent ripple-flow. There is no rooting or soil development. Their lateral extent is dependent on their depositional environment interpretation: interfluvial settings (may be extensive if multiple point sources of sediment); margins of a playa lake (more extensive than interfluve); or stratigraphic surface associated with shifts in climate or sediment supply. The sedimentological interpretation of the extent of possible baffles at Endurance was incorporated into the static model via variograms. A range was included in these variograms and sensitivities tested.

The petrophysical model was created to provide the rock property inputs to the static model. The petrophysical model used data from the three wells drilled on structure, supplemented with off-structure wells to provide appropriate property ranges. The mean average properties on structure indicate that the Bunter Sandstone is a very high net to gross system, with good porosity and permeability reservoir quality. Expected parameter ranges (P10 – Mean – P90) are: net-to-gross 74 – 95 – 97%; porosity 16.4 – 22.5 – 24.1% and permeability 100 – 300 – 500mD (based on net reservoir cut-offs of $V_{cl} < 0.2$ and porosity > 0.1). Outside of structure (and

seismic phase reversal), wells show varying degrees of halite cementation that can be flagged from log data. The effect on porosity has been mapped out and included in the static model.

A set of models that captures the agreed uncertainty framework (overall level of vertical and horizontal heterogeneities) and honours the dynamic data gathered in well 42-25d-3 was built in Petrel. This incorporates insights from the sedimentological core lithotype study, reprocessed seismic data and regional analogues. Emphasis has been placed in building a fine grid that could capture the vertical heterogeneities observed in the core: in most cases, these heterogeneities are less 1m thick and commonly just a few tens cm in vertical thickness. Therefore, a fine-scale grid (geomodel) at near log scale resolution was built to model these heterogeneities (30 cm in average vertically). Four petrofacies (cemented sandstone, partially cemented sandstone, good-quality sandstone, and heterolithics), were derived from wireline log cut-off criteria have been generated and have been distributed across the reservoir through the two regions to define the gross areas of cemented and un-cemented rock based on the seismic phase reversal (SPR) at the Top Bunter Sandstone horizon.

In addition to the 4 petrofacies defined by wireline log cut-off criteria, five additional potentially continuous baffled zones (of varying degrees of confidence) were identified in cores. These have been hard-wired into the grid, and the uncertainty in lateral extent has been addressed by modelling with different variograms per facies and variable net-to-gross levels resulting in three discrete static models.

Porosity has been modelled thereafter through a gaussian simulation process in Petrel. Permeability was directly calculated from modelled porosity with a porosity-permeability transform derived from core data from wells 42/25-1 and 42/25d-3. The porosity-permeability transform has been adjusted to ensure that the simulation model (coarse model) do match the dynamic permeability observed from the well test in 42/25d-3.

Reservoir properties were upscaled back to coarse-scale model (simulation grid) using a flow-based upscaling algorithm in Petrel. Upscaling quality assurance has been carried out for both static properties (volumetric checks) and permeability field (single-phase tracer modelling).

7.0 References

- Bachmann G.H., Geluk, M.C., Warrington, G., Becker-Roman, A., Beutler, G., Hagdom, H., Hounslow, M.W., Nitsch, E., Rohling, H.G., Simon, T. and Szulc, A., 2010. Triassic. In: J.C. Doornenbal and A.G. Stevenson (Eds.) Petroleum Geological Atlas of the Southern Permian Basin Area, EAGE Publications, Houten, 149–173.
- Blackbourn, G.A., 2012. Petrography of seven core samples from the Bunter Sandstone of well 42/25-1, UK North Sea. Blackbourn Geoconsulting, report prepared for National Grid Carbon in consultation with AGR Petroleum Services, 35pp.
- Blackbourn, G.A., 2014. Petrography of cuttings samples from the Bunter Sandstone of well 43/28a-3, UK North Sea. Blackbourn Geoconsulting, report prepared for National Grid Carbon in consultation with AGR Petroleum Services, 46pp.
- Blackbourn, G.A. and Robertson, L.F., 2014. Sedimentology, petrography and burial history of the cored Triassic section in National Grid Carbon well 42/25d-3, UK North Sea. Blackbourn Geoconsulting, report prepared for National Grid Carbon in consultation with AGR Petroleum Services, 163pp.
- Conway, A.M. and Valvatne, C., 2003. The Boulton Field, Block 44/21a, UK North Sea. In: J.G. Gluyas and H.M. Hitchens (Eds.) United Kingdom Oil and Gas Fields Commemorative Millennium Volume, Geological Society, London, Memoir, 20, 671–680.
- Coward, M.P., Dewey, J., Hempton, M. and Holroyd, J., 2003. Tectonic evolution. In: D. Evans, C. Graham, A. Armour and P. Bathurst (Eds.) The Millennium Atlas: Petroleum Geology of the Central and Northern North Sea, Geological Society, London, 17–23.
- Doornenbal, J.C. and Stevenson, A.G. (Eds.), 2010. Petroleum Geological Atlas of the Southern Permian Basin Area, EAGE Publications, Houten, 342pp.
- Gast, R.E., Dunsar, M., Breikreuz, C., Gaupp, R., Schneider, J.W., Stemmerik, L., Geluk, M.C., Geisbler, M., Kiernsnowski, H., Glennie, K.W., Kabel, S. and Jones, N.S., 2010. Rötlied. In: J.C. Doornenbal and A.G. Stevenson (Eds.) Petroleum Geological Atlas of the Southern Permian Basin Area, EAGE Publications, Houten, 101–121.
- George, G.T. and Berry, J.K., 1997. Permian (Upper Rötlied) synsedimentary tectonics, basin development and palaeogeography of the southern North Sea. In: K. Ziegler, P. Turner and S.R. Daines (Eds.) Petroleum Geology of the Southern North Sea: Future Potential, Geological Society, London, Special Publication, 123, 31–61.
- Geluk, M., McKie, T. and Kilhams, B., 2018. An introduction to the Triassic: current insights into the regional setting and energy resource potential of NW Europe. In: B. Kilhams, P.A. Kukla, S. Mazur, T. McKie, H.F. Munlieff and K. Van Ork (Eds.) Mesozoic Resource Potential in the Southern Permian Basin, Geological Society, London, Special Publication, 469, 139–147.

- Glennie, K.W., 1997. History of exploration in the southern North Sea. In: K. Ziegler, P. Turner and S.R. Daines (Eds.) *Petroleum Geology of the Southern North Sea: Future Potential*, Geological Society, London, Special Publication, 123, 5–16.
- Grant, R.J., Underhill, J.R., Hernandez-Casado, J. and Barker, S., 2019. Upper Permian Zechstein Supergroup carbonate-evaporite platform palaeomorphology in the UK Southern North Sea, *Marine and Petroleum Geology*, 100, 484–518.
- Guterch, A., Wybraniec, S., Grad, M., Chadwick, R.A., Krawczyk, C.M., Zeigler, P.A., Thybo, H. and De Vos, W., 2010. Crustal structure and structural framework. In: J.C. Doornenbal and A.G. Stevenson (Eds.) *Petroleum Geological Atlas of the Southern Permian Basin Area*, EAGE Publications, Houten, 11–23.
- Kombrink, H., Besly, B.M., Collinson, J.D., Den Hartog Jager, D.G., Drozdrewski, G., Dunsar, M., Hoth, P., Pagnier, H.J.M., Stemmerik, L., Waksmundzka, M.I. and Wrede, V., 2010. Carboniferous. In: J.C. Doornenbal and A.G. Stevenson (Eds.) *Petroleum Geological Atlas of the Southern Permian Basin Area*, EAGE Publications, Houten, 81–99.
- Leppard, R., 2011. Regional model building for an aquifer storage system in the Bunter Formation: sedimentology study. Leppard Sedimentology Report No. 85/11, prepared for National Grid Carbon Ltd, 32pp.
- Lott, G.K., Wong, T.E., Dunsar, M., Andsbjerg, J., Monnig, E., Feldman-Olszewska, A. and Verreussel, R.M.C.H., 2010. Jurassic. In: J.C. Doornenbal and A.G. Stevenson (Eds.) *Petroleum Geological Atlas of the Southern Permian Basin Area*, EAGE Publications, Houten, 175–193.
- Moscariello, A., 2003. The Schooner Field, Blocks 44/26a, 43/30a, UK North Sea. In: J.G. Gluyas and H.M. Hichens (Eds.) *United Kingdom Oil and Gas Fields, Commemorative Millennium Volume*, Geological Society, London, Memoir, 20, 811–824.
- O'Mara, P.T., Merryweather, M., Stockwell, M. and Bowler, M., 2003. The Trent Gas Field, Block 43/24a, UK North Sea. In: J.G. Gluyas and H.M. Hichens (Eds.) *United Kingdom Oil and Gas Fields, Commemorative Millennium Volume*, Geological Society, London, Memoir, 20, 835–849.
- Pharaoh, T.C., Dunsar, M., Geluk, M.C., Kockel, F., Krawczyk, C.M., Krzywiec, P., Scheck-WendeRöth, M., Thybo, H., Vejbaek, O.V. and Van Wees, J.D., 2010. Tectonic evolution. In: J.C. Doornenbal and A.G. Stevenson (Eds.) *Petroleum Geological Atlas of the Southern Permian Basin Area*, EAGE Publications, Houten, 25–57.
- Richardson, S., 2015. Key structural elements, tectonostratigraphy and lineament analysis of the Southern North Sea. BP internal report, 40pp.
- Stewart, S.A. and Coward, M.P., 1995. Synthesis of salt tectonics in the southern North Sea, UK, *Marine and Petroleum Geology*, 12 (5), 457–475.

Underhill, J.R., 2003. The tectonic and stratigraphic framework of the United Kingdom's oil and gas fields. In: J.G. Gluyas and H.M. Hitchens (Eds.) United Kingdom Oil and Gas Fields, Commemorative Millennium Volume, Geological Society, London, Memoir, 20, 17–59.

White Rose, 2016. K40: Subsurface geoscience and production chemistry reports. Capture Power Limited, 300pp.,
https://assets.publishing.service.gov.uk/government/uploads/system/uploads/attachment_data/file/531045/K40_Subsurface_Geoscience_and_Production_Chemistry.pdf

This publication is available from: www.gov.uk/beis

If you need a version of this document in a more accessible format, please email enquiries@beis.gov.uk. Please tell us what format you need. It will help us if you say what assistive technology you use.